Estimating CO_2 Leakage Fluxes along Legacy Wells Using a Rapid Physics-Based Screening Approach

Hariharan Ramachandran [1*], Iain de Jonge-Anderson [1,2], Benjamin Pullen [3], Aaron Cahill [3]

[1] Institute of GeoEnergy Engineering, Heriot-Watt University, Edinburgh, UK
[2] Department of Civil & Environmental Engineering, University of Strathclyde,
Glasgow, UK
[3] Lyell Centre, Heriot-Watt University, Edinburgh, UK

* Correspondence: Hariharan Ramachandran, h.ramachandran@hw.ac.uk
ORCiD: 0000-0001-5979-0930 (HR)

Estimating CO_2 Leakage Fluxes along Legacy Wells Using a Rapid Physics-Based Screening Approach

Hariharan Ramachandran [1]*, Iain de Jonge-Anderson [1,2], Benjamin Pullen [3], Aaron Cahill [3]

[1] Institute of GeoEnergy Engineering, Heriot-Watt University, Edinburgh, UK

[2] Department of Civil & Environmental Engineering, University of Strathclyde, Glasgow, UK

[3] The Lyell Centre, Heriot-Watt University, Edinburgh, UK

* Correspondence: Hariharan Ramachandran, H.Ramachandran@hw.ac.uk

ORCiD: 0000-0001-5979-0930 (HR)

Abstract

Achieving net-zero targets demands the rapid expansion of CO_2 geological storage, but legacy wells in mature petroleum provinces represent a significant containment risk when engineered barriers degrade. At the early assessment stage, storage projects need to rapidly bound plausible leakage magnitudes across large legacy-well inventories when integrity data are sparse; however, suitable modelling approaches remain limited. High-fidelity simulations capture leakage physics in detail but are computationally demanding, while simpler analytical models neglect depth-dependent CO_2 property variations arising from realistic pressure–temperature gradients. We present QWellRATE, a simplified physics-based screening model for rapidly estimating upper-bound steady-state CO_2 leakage fluxes along legacy wellbore pathways. The model evaluates depth-dependent CO_2 density and viscosity using the Span–Wagner equation of state, represents leakage pathways as an equivalent Darcy continuum, and operates on readily available inputs without requiring coupled reservoir simulation. Predicted flux magnitudes are consistent with published field analogues from abandoned wells across configurations ranging from intact multi-plug systems to unplugged pathways. Cement plug permeability is the primary control on leakage flux: two intact cement plugs reduce flux by approximately 760-fold relative to an unplugged well, while simultaneous degradation of all three plugs produces an approximately 500-fold increase. The model's computational efficiency enables sensitivity analysis, uncertainty quantification, and regional spatial screening. Uncertainty quantification via Latin Hypercube Sampling yields a five-order-of-magnitude flux range driven by multiplicative interactions between degraded cement and elevated mud permeability. Regional demonstration in the Southern North Sea illustrates how QWellRATE can support tiered workflows by prioritising legacy wells for targeted follow-up using high-fidelity multiphase simulators.

Keywords: CO_2 storage, wellbore leakage, legacy wells, flux assessment, uncertainty quantification, reduced complexity models

1. Introduction

Limiting global warming to well below 2 °C by 2100 requires rapid, deep, and sustained reductions in greenhouse gas emissions (Krevor et al., 2023; Riahi et al., 2023). Achieving this goal depends partly on the widespread deployment of CO_2 geological storage (CGS) at gigatonne scales over the coming decades (Riahi et al., 2023). This expansion demands efficient and reliable methods for evaluating the suitability and containment security of candidate storage complexes. Such assessments must account not only for the intrinsic geological properties of the storage formation and overburden but also for risks to long-term containment posed by pre-existing infrastructure, particularly legacy wells from prior hydrocarbon operations.

Legacy wells, historical boreholes drilled and later abandoned within potential CGS sites, represent one of the most significant threats to storage integrity when engineered barriers fail, creating pathways for upward fluid migration (King & Valencia, 2014). This risk is especially pertinent in mature petroleum provinces such as the UK North Sea and the Gulf of Mexico, which offer ideal geological and infrastructural conditions for early-stage CGS yet also host exceptionally dense well networks (Nicot, 2009; Pullen et al., 2025). In these regions, well densities commonly exceed one per km^2, and field investigations have documented measurable leakage at a non-trivial fraction of abandoned wells, ranging from 10 - 25 % offshore (Davies et al., 2014) and as high as 30 - 50 % onshore according to some investigations (Bowman, 2023; Cahill et al., 2023). Although most wells remain effectively sealed, low individual failure probabilities translate to substantial cumulative risk across thousands of wells (e.g., Lackey et al., 2019; Lackey et al., 2021). These observations underscore the need for robust, scalable methods to assess potential leakage and prioritize wells that require closer scrutiny.

This study targets the screening and triage stage of CO_2 storage assessment workflows, where the objective is to rapidly bound plausible leakage magnitudes across large populations of legacy wells under uncertainty. It does not aim to resolve leakage pathway identification or detailed multiphase reservoir–well dynamics, which are typically addressed using site-specific models at later stages. Instead, the focus is on deriving physically defensible upper-bound leakage flux estimates suitable for prioritisation and comparative assessment. These estimates are upper bounds by construction: the model assumes single-phase CO_2 flow following complete displacement of the aqueous phase and neglects capillary resistance along the pathway, such that any residual two-phase or capillary effects in reality would act to reduce the predicted flux (Section 2.2).

The integrity of any legacy wellbore depends on a sequence of engineered barriers installed during both the original completion and later plug-and-abandonment (P&A) phases. During completion, steel casing and annular cement are intended to hydraulically isolate formations and provide structural support. During abandonment, additional cement plugs or mechanical barriers are emplaced at specified intervals to ensure long-term zonal isolation once production ceases (Nelson, 1990; Vrålstad et al., 2019; Khalifeh & Saasen, 2020; Chukwuemeka et al., 2023). In practice, barrier design, placement, and quality vary widely across regulatory regimes and historical eras. Consequently, integrity loss can occur through two broad mechanisms: intrinsic degradation of the original or abandonment materials (e.g., corrosion, shrinkage, or chemical attack) and extrinsic deficiencies such as poor placement, incomplete cement returns, or mechanical failure induced by stress cycling (Watson & Bachu, 2009; Zhang & Bachu, 2011; Kiran et al., 2017; Arild et al., 2018). Once barriers are compromised, pressure gradients could drive CO_2 migration along annuli, fractures, or cement defects, thereby compromising long-term storage containment.

Predictive modelling plays a critical role in quantifying plausible leakage fluxes under different integrity-failure scenarios, providing essential input to risk-management frameworks and site-selection decisions. A variety of modelling approaches has been developed, spanning a wide range of computational complexity and physical fidelity. High-fidelity numerical simulations (e.g., Zhou et al., 2005; Zhang et al., 2007; Kopp et al., 2010; Humez et al., 2011; Harp et al., 2014; Pan and Oldenburg, 2014; Lu and Connell, 2014; Yang et al., 2019; Johnson et al., 2021; Cai et al., 2022; Moghadam et al., 2023) explicitly resolve multiphase, non-isothermal flow and detailed wellbore-reservoir coupling, offering rich process understanding but at considerable computational cost. To improve tractability, analytical and semi-analytical models have been developed that idealise flow physics and geometry, enabling rapid estimation of steady-state leakage fluxes (Nordbotten et al., 2005, 2009; LeNeveu, 2008; Celia et al., 2011; Pan et al., 2011). These formulations provide first-order insights but assume isothermal conditions. Further simplification has been achieved through reduced-order models (ROMs) that emulate the behaviour of more complex simulators by identifying dominant controls and parameter sensitivities (Jordan et al., 2015; Harp et al., 2016; Keating et al., 2016; Zheng et al., 2014; Mehana et al., 2020; Gan et al., 2021).

Complementary screening methodologies and system-level frameworks have also emerged to integrate these modelling tools within broader storage assessment workflows (Viswanathan et al., 2008; Vasylkivska et al., 2021; Bump et al., 2023; Arbad et al., 2024; Pullen et al., 2025; Smith et al., 2026). Among these, system-level frameworks such as NRAP-Open-IAM (Vasylkivska et al., 2021) represent the most established approach to integrated storage risk assessment; however, their wellbore leakage components are built on isothermal formulations (Nordbotten et al., 2009; Harp et al., 2016) and require transient pressure and saturation inputs from a coupled reservoir model, positioning them at a later, data-rich stage of assessment where site-specific reservoir simulation outputs are already available, leaving a complementary need unmet at the earlier screening stage. This landscape reveals a clear gap: existing analytical models are computationally efficient but physically oversimplified, while high-fidelity simulators capture relevant physics but are impractical for screening hundreds to thousands of wells. What is needed is a middle ground - a tool that retains essential physics governing CO_2 leakage while enabling rapid evaluation across large well populations and uncertain parameter spaces.

Here, we address this need by applying a simplified, physics-based model (QWellRATE) to estimate upper bounds on CO_2 leakage fluxes along integrity-compromised legacy wells under non-isothermal conditions. The model (i) represents the leakage pathway as an equivalent Darcy continuum, (ii) explicitly incorporates depth-dependent thermophysical properties of CO_2 (Span & Wagner, 2003a, 2003b), and (iii) operates on readily available well and reservoir inputs, enabling rapid scenario analysis, sensitivity studies, and uncertainty quantification across large well inventories. We use the model to interrogate key controls (e.g., plug permeability and length, pathway effective permeability, pressure regime, geothermal gradient and depth), quantify how barrier degradation affects flux, and demonstrate a regional scenario in the Southern North Sea to illustrate prioritisation of wells for detailed assessment. The approach is intended for screening and comparative prioritisation; flagged wells can then be evaluated with high-fidelity simulators that resolve transient multiphase flow and chemo-mechanical interactions.

2. Methods

2.1 Conceptual framework

This section presents the conceptual framework underpinning QWellRATE for estimating CO_2 leakage fluxes along legacy wellbore pathways at the screening stage of a CO_2 storage assessment workflow (e.g., Pullen et al., 2025). We adopt a simplified formulation that balances computational efficiency with physical realism, accepting reduced process fidelity as appropriate for screening-level assessment across large well inventories and uncertain parameter spaces.

We consider the scenario in which a CO_2 plume intersects a compromised wellbore pathway, driving upward migration from the storage reservoir to the surface or seafloor along the wellbore (Figure 1). These pathways include damaged casing, cement plugs and open-hole intervals, and degraded annular cement, all of which are represented within the equivalent continuum framework described below. Pressure equilibration in wellbore-scale systems occurs over days to weeks, substantially shorter than storage project timescales (years to decades). We therefore decouple reservoir-scale processes, where multiphase CO_2–brine flow governs plume migration, trapping, and pressure evolution, from wellbore-scale processes by assuming the CO_2 plume has reached and fully saturated the wellbore base, reducing the problem to steady-state leakage along the wellbore pathway. The reservoir is consequently idealised as a constant-pressure, constant-temperature CO_2 source at the lower boundary of the wellbore. Within the pathway, we assume CO_2 has displaced the aqueous phase to residual saturation following breakthrough, establishing single-phase CO_2 flow conditions that persist during long-term leakage. The upper boundary is set at the surface, seafloor, or a specified shallow horizon such as a groundwater aquifer. For surface terminations, atmospheric pressure and ambient temperature are prescribed; for seafloor or shallow aquifer terminations, the corresponding hydrostatic pressure and local geothermal temperature are applied. The wellbore is treated as impermeable to lateral flow, with vertical CO_2 migration governed by the pressure gradient and the gravitational contribution of the CO_2 column.

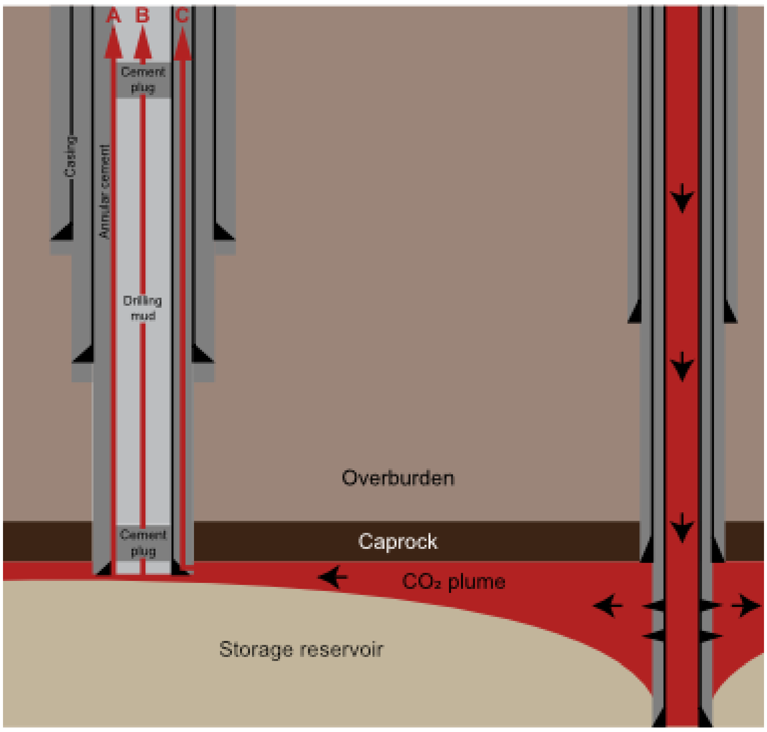

Figure 1: Schematic illustration of a legacy well (left) and CO_2 injection well (right) with potential leakage pathways annotated. A: leakage via damaged casing, B: leakage via cement plugs and open hole, C: leakage via damaged annular cement.

Real wellbore leakage occurs along intricate, heterogeneous pathways including microfractures, cylindrical channels, and micro-annuli within the casing-cement system (Gasda et al., 2004; Moeinikia et al., 2018). In degraded cement specifically, flow is rarely matrix-controlled: microfractures, microannuli at casing-cement and cement-formation interfaces, and channels formed during placement constitute the dominant flow pathways (Kiran et al., 2017). We therefore represent these pathways as an equivalent Darcy continuum characterised by an effective permeability, consistent with established practice in wellbore leakage modelling (Celia et al., 2011; Tao et al., 2010, 2014; Harp et al., 2016). Direct leakage measurements or sustained casing pressure (SCP) data are used to back-calculate the effective permeability of these pathways by combining pressure and flow observations with Darcy-based simulations (Huerta et al., 2009; Checkai et al., 2013; Tao et al., 2014). Where direct measurements are unavailable, permeability can be inferred from analogous wellbore studies or laboratory data on cement and casing defects (Bachu & Bennion, 2009; Carey et al., 2010; Harooni et al., 2025). The effective permeability adopted here is therefore an integrated measure of these features, implicitly encoding fracture aperture, fracture density, and connectivity at the scale of the barrier element, rather than a property of the intact cement matrix. Compilations spanning intact to severely degraded states report effective cement permeabilities ranging across six to twelve orders of magnitude (Torsæter et al., 2024), and the distributions adopted in Section 3.4 (10^{-12} to 1 D) are chosen to span this range, including fracture-dominated states. What the equivalent-continuum treatment does not resolve is the evolution of individual fracture properties, including aperture changes under effective stress, and reactive opening or self-sealing under CO_2-charged conditions. Capturing these processes requires coupled chemo-mechanical models at the site-specific stage (Iyer et al., 2018; Yang et al., 2019).

The leakage pathway is simplified as a one-dimensional vertical porous medium, which is appropriate given that wellbore length (hundreds to thousands of metres) greatly exceeds its diameter (tens of centimetres), making lateral property gradients negligible relative to the axial flow resistance. The pathway is defined by averaged properties (porosity, permeability) and geometric parameters that determine cross-sectional flow area. For annular pathways, the flow area depends on casing diameter and annular gap width; for fractures, it depends on aperture and extent; for channels, it depends on equivalent radius. Along-well property variations, such as alternating mud and cement column segments, are captured through these averaged values, whereas complex pathway characteristics including stress-dependent properties, and detailed cement fracture network geometry are not explicitly represented. This simplification is appropriate for screening-level assessment where population-scale coverage takes precedence over geometric detail.

2.2 Governing equations and model assumptions

QWellRATE employs several simplifying assumptions to enable computational efficiency while producing upper-bound estimates of leakage flux, consistent with the design philosophy of a screening tool intended to avoid false negatives when prioritising wells for detailed assessment. The physical basis and directional bias of each assumption are discussed below, followed by the governing equation.

Pathway walls are assumed impermeable, limiting fluid flow to the vertical direction. This is appropriate when cement sheaths and casing provide effective hydraulic isolation, as intended by construction standards and demonstrated experimentally (Carey et al., 2010; Bachu & Bennion, 2009). However, QWellRATE cannot represent scenarios where debonding, fractures, or permeable interfaces allow CO_2 diversion into adjacent formations (thief zones), potentially reducing surface leakage (Harp et al., 2014). Setting CO_2 relative permeability to unity (k_{rg} = 1.0), consistent with the single-phase flow assumption established in Section 2.1, provides upper-bound flux estimates; actual fluxes under two-phase conditions would be lower due to relative permeability reduction, typically by factors of two to ten or more depending on saturation history (Bachu & Bennion, 2009; Baek et al., 2023). Neglecting capillary resistance removes an additional entry-pressure barrier that would otherwise delay or prevent CO_2 migration through fine-grained barrier materials, further biasing flux estimates upward.

Unlike prior semi-analytical formulations for wellbore leakage (e.g., Nordbotten et al., 2005; Celia et al., 2011), which assume isothermal conditions, QWellRATE evaluates depth-dependent CO_2 density and viscosity capturing the thermophysical property variations that arise across realistic wellbore pressure - temperature profiles. Pathway temperature is assumed to be in thermal equilibrium with the surrounding geothermal temperature at the depth. This assumption neglects the advective heat transport, conductive heat losses and Joule-Thomson cooling, thereby simplifying the thermal transport and avoiding the need to solve energy conservation. The local temperature is used to evaluate depth-dependent CO_2 density and viscosity, which are used in the mass balance equation (Equation 1). This is reasonable for typical wellbore geometries where radial heat exchange with surrounding rock occurs faster than vertical CO_2 migration. Well-cemented pathways with thermal contact to formations maintain near-geothermal temperatures (Pan & Oldenburg, 2014; Lu & Connell, 2014). However, for very high flux or extensive pressure drops, Joule-Thomson cooling may cause the model to overestimate flux (Lu & Connell, 2014; Cai et al., 2022).

Each simplification carries a known direction of bias relative to the full-physics problem, and together they define the upper-bound character of the model. Assuming single-phase CO_2 flow with complete aqueous-phase displacement overestimates flux relative to two-phase conditions, where relative permeability reduction would lower CO_2 mobility. The steady-state idealisation is appropriate for long-term leakage assessment: although pressure equilibration within the wellbore pathway occurs over days to weeks, the steady rate represents the sustained flux once equilibration is established, providing an upper bound on time-averaged leakage over storage project timescales. Treating pathway walls as impermeable excludes diversion into thief zones, which field and modelling studies show can substantially reduce flux reaching the surface (Harp et al., 2014), causing surface flux to be overestimated. The thermal-equilibrium assumption is the only simplification that introduces bias in either direction, overestimating flux where Joule-Thomson cooling would otherwise reduce CO_2 mobility at high rates (Lu & Connell, 2014; Cai et al., 2022). The net effect is that QWellRATE systematically errs toward higher fluxes, which is the appropriate failure mode for a screening tool whose purpose is to avoid false negatives when prioritising wells for detailed assessment.

These simplifications exclude transient plume migration at the reservoir scale and within the wellbore pathway, multiphase flow, open wellbore flow, capillary trapping, and chemical interactions between CO_2 and wellbore materials such as cement degradation. These processes can significantly influence leakage rates and should be addressed in site-specific analyses (Gasda et al., 2004; Huerta et al., 2009; Celia et al., 2011; Harp et al., 2016; Arzanfudi & Al-Khoury, 2017; Iyer et al., 2018; Yang et al., 2019; Baek et al., 2023; Baek et al., 2025; Kim et al., 2025). Given these assumptions, QWellRATE is most appropriately applied for screening large well populations and comparative scenario analysis rather than predicting precise leakage rates at individual wells. High-priority wells identified at this stage should be advanced to high-fidelity multiphase simulators for detailed assessment.

For steady-state, single-phase vertical flow in a 1D porous medium, mass conservation requires constant mass flux along the pathway:

$$\frac{dm}{dz} = 0, where\ m = -\frac{\rho_g kA}{\mu_g}\left(\frac{dP}{dz} - \rho_g g\right) \tag{1}$$

where m is the total mass rate (kg s^{-1}), A is the flow area (m^2), k is the effective permeability (m^2), μ_g is the CO_2 viscosity (Pa s), g is the gravitational acceleration (9.81 ms^{-2}) and ρ_g is the CO_2 mass density (kg m^{-3}). Relative permeability does not appear because k_{rg} is assumed to be 1 for single-phase flow at residual aqueous saturation; k therefore represents the effective permeability to CO_2 under these conditions. The leakage flux is obtained by dividing the mass rate (m) by the flow area (A). The pathway is discretized into blocks, and the coupled pressure and flux equations are solved iteratively using a finite volume approach until the mass balance residual is below tolerance (10^{-9}). QWellRATE is implemented in the Julia programming language (Bezanson et al., 2017), full details and source code are available on Zenodo (Ramachandran et al., 2025), and its verification is provided in Appendix A.

2.3 Thermophysical properties

Within the governing equation framework established in Section 2.2, the primary source of physical complexity is the depth-dependent variation of CO_2 thermophysical properties along the wellbore. CO_2 density and viscosity vary substantially as pressure and temperature decrease from reservoir conditions at the wellbore base to surface or seafloor conditions at the upper boundary. Under representative storage conditions, this pressure–temperature decline produces large contrasts in CO_2 density along the wellbore, with values differing by more than an order of magnitude between reservoir depth and the surface or seafloor. Neglecting these variations, as isothermal formulations do, introduces systematic errors in predicted flux that become particularly pronounced near the CO_2 critical point (304.1 K, 7.38 MPa), where small changes in pressure or temperature produce large changes in density.

QWellRATE evaluates CO_2 density and viscosity at each depth node using the Span–Wagner multi-parameter equation of state (EOS) (Span & Wagner, 2003a, 2003b), which uses 12 empirically fitted parameters and demonstrates accuracy across the full range of pressure–temperature conditions encountered during typical storage operations (Böttcher et al., 2012). Pressure is related to density and temperature through the dimensionless Helmholtz free energy (a) as:

$$P = \rho RT(1 + \delta\alpha_\delta^r), \tag{2}$$

where P is the pressure (MPa), ρ is the mass density (kg m^{-3}), R is the specific gas constant (0.1889241 kJ kg^{-1} K^{-1}), T is the temperature (K), δ is the reduced density ($\delta = \rho/\rho_c$), ρ_c is the critical density (467.6 kg m^{-3}), τ is the inverse reduced temperature ($\tau = T_c/T$), T_c is the critical temperature (304.1282 K), P_c is the critical pressure (7.3773 MPa), α is the dimensionless Helmholtz energy ($\alpha = a/RT$), α^r_δ is the partial derivative of the real part (r) of the dimensionless Helmholtz energy with respect to reduced density. Full details of the equation formulation are given in Span & Wagner (2003a, 2003b). CO_2 viscosity is evaluated using a corresponding states model (Vesovic et al., 1990; Fenghour et al., 1998). Together, these property evaluations are performed at each depth along the discretised wellbore pathway, providing the depth-dependent inputs to the mass balance equation (Equation 1) at each iteration of the finite volume solver.

3. Results and Discussion

3.1 Impact of cement plug position and permeability on leakage fluxes

We analyse CO_2 leakage along legacy wellbores using three synthetic scenarios that represent a progression of abandonment practice documented in the plug and abandonment literature (Figure 2). Scenario (a) represents a well with no cement plugs, where a uniform effective permeability of 0.01 mD reflects the permeability of heavy drilling mud throughout the pathway, representative of wells abandoned prior to formal plugging requirements (Tao & Bryant, 2014). Scenario (b) incorporates two 50 m cement plugs positioned at 300 mbsf (20 % of total depth) and at 1200 mbsf (80 % of total depth), isolating the shallow and reservoir intervals respectively. This configuration reflects pre-standardisation practice, where plugs were placed at key isolation intervals without codified length or count requirements. Scenario (c) adds a third 50 m plug at 50 % of total depth (750 mbsf), providing an additional mid-depth barrier consistent with modern abandonment standards requiring multiple plugs of at least 50 m, as codified from 2004 onward (Torsæter et al., 2024; Vrålstad et al., 2019). For scenarios (b) and (c), cement plug permeability is set to 1 nD, representative of intact Class G Portland cement (Bachu & Bennion, 2009), while non-cemented intervals retain the 0.01 mD effective permeability of scenario (a). Table 1 summarises the reference simulation parameters. The flux differences between scenarios therefore have direct implications for how wells of different abandonment eras should be prioritised in regional screening workflows.

Table 1 – Simulation information for the well leakage system. See Figure 2 for a schematic representation. (a), (b) and (c) refer to the respective labelling on Figure 2.

Parameter	Reference value
Effective mud permeability (mD)	0.01
Reservoir depth (mbsf)	1500
Geothermal gradient (K km^{-1})	30
Seafloor temperature (K)	293.15
Seafloor depth (mbsl)	100
Number of cement plugs	0 (a) ,2 (b) ,3 (c)
Plug permeability (D)	1x10^{-9}
Plug thickness (m)	50

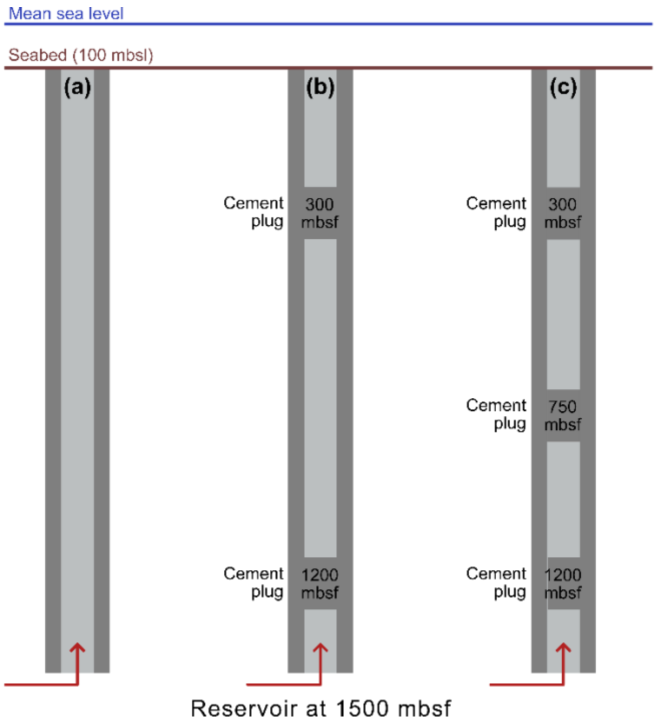

Figure 2 – Conceptual models illustrating three distinct legacy wellbore configurations for CO_2 leakage analysis: (a) pathway with uniform permeability; (b) two-plug system sealing shallow and reservoir intervals; (c) three-plug system with additional mid-depth barrier, representative of legacy abandonment configurations documented in UK well records. All scenarios simulate offshore leakage from a storage reservoir at 1500 mbsf at 100 mbsl. Cement plugs (dark gray) have a permeability of 1 nD; non-cemented intervals (light gray) have a permeability of 0.01 mD. See Table 1 for detailed input parameters.

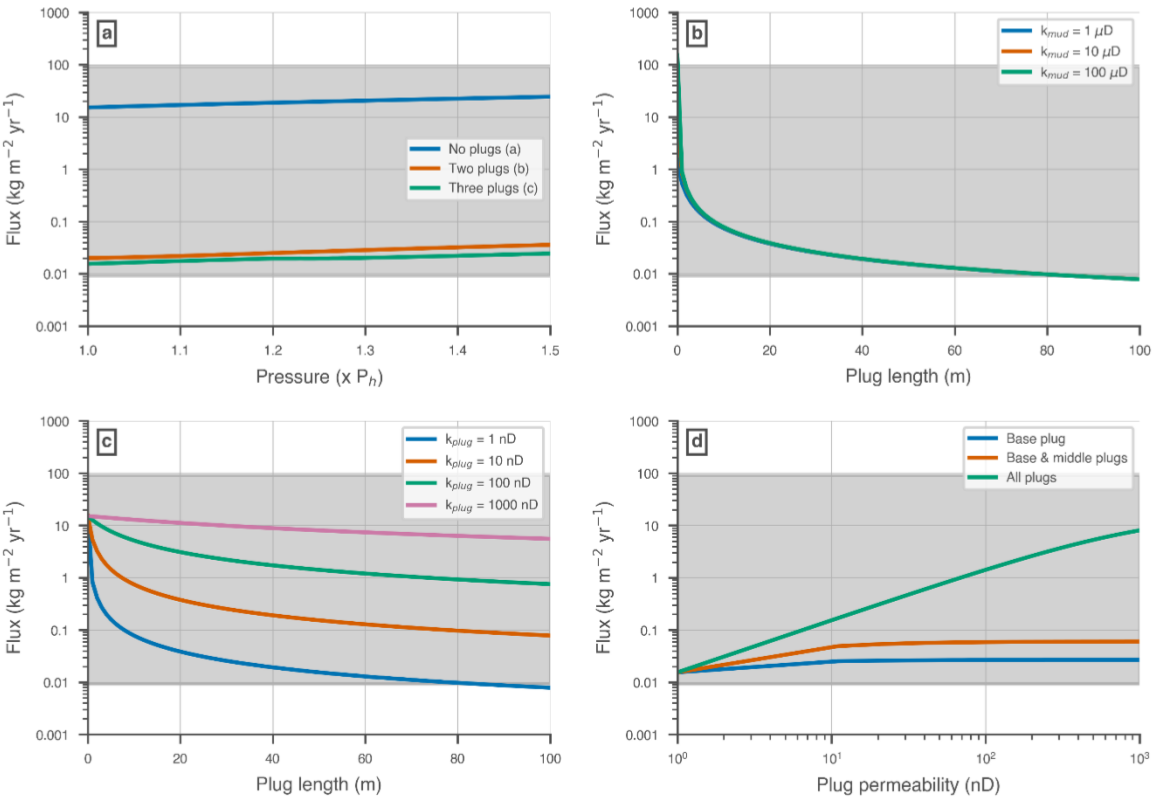

Figure 3 – CO_2 leakage flux sensitivity to wellbore configuration and plug properties. a – the leakage flux as a function of normalized pressure for the three conceptual wellbore scenarios as illustrated in Figure 2. b – Leakage flux as a function of cement plug length for scenario (c), evaluated across three effective permeabilities of the non-plugged intervals, with a constant plug permeability of 1 nD. c – Leakage flux as a function of cement plug length for scenario (c), explored with four plug permeabilities and a constant effective permeability of 0.01 mD for non-plugged intervals. d – Leakage flux as a function of increasing plug permeability, simulating degradation severity, for a fixed plug length of 50 m within scenario (c). The gray shaded area depicts measured leakage fluxes from Forde et al. (2019). Refer to Table 1 for input parameters.

Reservoir pressure during CO_2 storage evolves from elevated injection pressures toward near-hydrostatic conditions in the post-injection period. To illustrate, consider a post-injection scenario with a CO_2 column height of 10 m at the reservoir, giving a reservoir pressure $P_r = P_h + h\Delta\rho g$, where P_h is the hydrostatic pressure, h is the CO_2 column height, and $\Delta\rho$ is the density contrast between brine and CO_2 (assumed as 1000 and 600 kg m^{-3} respectively). This yields $P_r \approx 1.004 \times P_h$, indicating that even modest CO_2 accumulations produce small but non-negligible overpressure. This analysis considers reservoir pressures at or above hydrostatic; depleted pressures are not examined here. All reservoir pressures are normalised as multiples of hydrostatic pressure, with leakage flux calculated as a function of this normalised pressure (Figure 3). For the reference conditions in Table 1, normalised pressure values of 1.0 to 1.5 correspond to reservoir pressures of 15 MPa to 22.5 MPa, spanning the range expected during active CO_2 injection.

Figure 3a shows leakage flux as a function of normalised pressure for the three wellbore scenarios. All scenarios show increasing flux with rising reservoir pressure, reflecting the greater driving force for CO_2 migration. The addition of two cement plugs in scenario (b) reduces leakage flux by approximately 760-fold relative to scenario (a) across the normalised pressure range of 1.0 to 1.5, illustrating the dominant role of engineered barriers over mud-fill permeability alone. Adding a third plug in scenario (c) produces a further 22 % reduction relative to scenario (b) across the full pressure range. This demonstrates a threshold effect in which initial barrier placement dramatically reduces leakage, but additional plugs yield progressively diminishing returns. For prioritisation purposes, the greatest flux reduction arises from the first two plugs; a well with two intact plugs carries substantially lower leakage risk than one with none, irrespective of whether additional plugs are present.

Figure 3b examines how cement plug length influences leakage flux for scenario (c), evaluating plug lengths from 0 to 100 m across three effective permeabilities of the non-cemented intervals (1 μD, 10 μD, 100 μD) for a fixed normalised pressure of 1.1. In the absence of any plug length (length = 0 m), leakage flux is equivalent to scenario (a) since no cement barriers are present and reaches approximately 150 kg m^{-2} yr^{-1} for the 100 μD case. Increasing plug length to 50 m produces a sharp, multi-order-of-magnitude flux reduction: for the 100 μD case, flux decreases to ~0.016 kg m^{-2} yr^{-1}, representing a transition from mud-dominated to plug-dominated flow resistance. Beyond 50 m, the flux curve plateaus, with extension from 50 to 100 m yielding less than a two-fold additional reduction. This plateau emerges because once plug length exceeds a critical threshold, plug permeability rather than length becomes the dominant flow resistance. Notably, this threshold of approximately 50 m corresponds directly to the minimum plug length required under modern abandonment standards codified from 2004 onward (Torsæter et al., 2024; Vrålstad et al., 2019), providing physical validation for that regulatory requirement. While the threshold cannot be considered an independent validation given that the scenario was designed around this plug length, the result confirms the physical basis for the standard. From a screening perspective, wells with plug lengths below approximately 50 m are the configurations most sensitive to any degradation in plug permeability and therefore warrant higher priority for follow-up assessment.

Figure 3c explores the interaction between plug length and permeability for scenario (c) at normalised pressure of 1.1. Plug permeability varies across three orders of magnitude (1 to 1000 nD) while holding pathway permeability constant at 0.01 mD. Plug permeability exerts dominant control: at 50 m length, reducing permeability from 1000 nD to 1 nD reduces flux by approximately 500-fold (from 8.1 to 0.016 kg m^{-2} yr^{-1}). Lower permeability plugs show greater sensitivity to length at short lengths (below 30 m) but plateau earlier as length increases, because at very low permeability even a short plug provides sufficient resistance to dominate system flow and additional length yields diminishing returns. Higher permeability plugs benefit more from extended length because accumulated resistance along the plug is required to compensate for the reduced per-unit resistance. This demonstrates that plug length acts as a buffer against the consequences of cement deterioration: wells with shorter plugs face disproportionately higher leakage risk under any degree of degradation, whereas longer plugs provide greater resilience against integrity loss. This analysis does not suggest that plug length compensates for poor cement quality. Rather, it highlights that plug length significantly modulates the severity of degradation-related leakage, providing essential information for prioritising wells requiring integrity assessment.

Figure 3d explores the impact of progressive cement plug degradation on leakage flux, using plug permeability as a proxy for damage severity, for scenario (c) with a fixed plug length of 50 m at normalised pressure 1.1. While cement plug deterioration may result from various chemical or mechanical processes, this study focuses exclusively on the consequent permeability enhancement as the primary parameter of interest. Three damage configurations are investigated: (1) degradation limited to the base plug only, (2) concurrent degradation of both the base and middle plugs, and (3) simultaneous degradation of all three plugs. When only the base plug degrades (Case 1), flux increases by less than 2-fold across the entire permeability range from 1 to 1000 nD (from 0.016 to 0.027 kg m^{-2} yr^{-1}), as the two intact upper plugs absorb virtually all of the additional driving force. Concurrent degradation of the base and middle plugs (Case 2) produces a similarly modest response, with flux increasing by less than four-fold across the same permeability range (from 0.016 to 0.060 kg m^{-2} yr^{-1}), as the single intact top plug continues to provide effective containment. The system becomes critically vulnerable only when all three plugs are simultaneously degraded (Case 3): flux increases by approximately 500-fold across the full permeability range (from 0.016 to 8.1 kg m^{-2} yr^{-1}), reaching within the same order of magnitude as an unplugged well under scenario (a). These results demonstrate that multi-plug systems provide redundancy against localised failures: individual or dual barrier degradation is almost entirely absorbed by the remaining intact plugs, and the system reaches critical vulnerability only when all barriers fail simultaneously.

3.2 Benchmarking QWellRATE against field analogues

We benchmark QWellRATE flux estimates against published field analogues to evaluate whether predicted magnitudes are empirically plausible across barrier-integrity states, while acknowledging differences in gas type, geometry, and site context between the model scenarios and available observations. Direct observations of CO_2 leakage from geological storage projects remain scarce; however, emissions of methane (CH_4) from plugged-and-abandoned legacy wells provide the most appropriate empirical analogue for assessing leakage through compromised wellbores. Broad compilations (e.g., Kang et al., 2014; Townsend-Small et al., 2016) report surface-flux ranges (~10^{-6}–10^{2} g m^{-2} s^{-1}) across mixed well types and integrity states. To benchmark QWellRATE under relevant conditions, we compared modelled CO_2 fluxes with direct wellhead-footprint measurements from plugged-and-abandoned wells where CH_4 and CO_2 emissions were quantified concurrently.

At two decommissioned wells in British Columbia, Cahill et al. (2023) measured excess CH_4 fluxes of 3–11 μmol s^{-1} and CO_2 fluxes of 150–476 μmol s^{-1}, corresponding to surface-emitted CH_4 rates of ~1.6–5.8 kg yr^{-1} and oxidation efficiencies exceeding 97 %. One of these sites (i.e. Wellsite J) was subsequently examined in greater detail by Cahill et al. (2025), who observed excess CH_4 and CO_2 fluxes of 55 and 867 μmol s^{-1} respectively, yielding a footprint-average surface CH_4 flux of ~1 kg m^{-2} yr^{-1} (~28 kg yr^{-1} total). These represent post-oxidation surface emissions (specifically, directly measured CH_4 efflux above established background concentrations) and therefore define lower bounds on total subsurface leakage, as a portion of CH_4 is oxidised before reaching the surface. Equivalent pre-oxidation fluxes, obtained by attributing excess CO_2 to fully oxidised CH_4 on a 1:1 molar basis, are provided in the Appendix B.

Additional field studies illustrate the breadth and variability of such emissions. Riddick et al. (2020) documented temporal variability in abandoned-well CH_4 fluxes from less than 1 mg h^{-1} to peaks near 80 g h^{-1} (~0.7 t yr^{-1} per well), while Forde et al. (2019) mapped spatial heterogeneity at the pad scale with surface CH_4 flux densities of 0.017–180 μmol m^{-2} s^{-1} (~0.009–91 kg m^{-2} yr^{-1}). Both datasets, also post-oxidation surface measurements, are used as contextual bounds rather than direct calibrations, collectively highlighting the strong spatial and temporal variability in real-world leakage, which QWellRATE's ensemble and uncertainty framework is designed to bracket rather than resolve at the individual well level. A further independent comparison is provided by Tao and Bryant (2014), who back-calculated effective leakage-path permeabilities (10 μD - 10 mD) from sustained casing pressure measurements across approximately 300 wellbores and computed worst-case steady CO_2 leakage fluxes, finding that over 90 % fell below 0.1 t m^{-2} yr^{-1}. The QWellRATE envelope for degraded configurations (Figure 3d) occupies the same range, despite one approach deriving permeability from sustained casing pressure data and the other from synthetic scenario analysis, providing independent support for the plausibility of the modelled values.

Across its configurations, QWellRATE predicts fluxes ranging from less than 0.01 to ~ 150 kg CO_2 m^{-2} yr^{-1}, ranging from an unplugged mud-filled pathway (scenario a) through two- and three-plug configurations (scenarios b and c) (Figure 3) as discussed in Section 3.1. This envelope overlaps the observed CH_4-analogue range, indicating that the model reproduces physically realistic flux magnitudes for wells of differing barrier integrity. Because CO_2 is denser, more viscous, and more soluble than CH_4, fluxes for equivalent permeability and pressure contrast are expected to fall at or below these CH_4-based analogues, consistent with QWellRATE's upper-bound design. Modelled magnitudes near the lower end approach the detection and measurement sensitivity of typical surface-flux monitoring systems (~10^{-5} g m^{-2} s^{-1}), implying that such low-flux leakage may remain unobservable at the surface and would instead require annular or subsurface monitoring.

Although the base simulations represent an offshore geometry with a 100 m water column, the governing parameters, i.e. permeability, pressure gradient, and barrier configuration, are general. The simulated flux magnitudes, therefore, provide a representative envelope for onshore legacy wells of comparable integrity class. We emphasise that this benchmarking tests whether predicted magnitudes are empirically plausible across barrier-integrity states; it does not constitute well-by-well predictive validation, which would require paired integrity and flux measurements that do not yet exist for CO_2 storage settings.

3.3 Sensitivity analysis

We conducted a one-at-a-time (OAT) sensitivity analysis using scenario (c) as the reference configuration to determine which input parameters most strongly influence predicted leakage fluxes and to identify which uncertainties carry the greatest weight for prioritisation decisions. Each parameter was systematically adjusted between defined minimum and maximum values (Table 2) while holding others constant at reference conditions. Results are presented as percentage deviation from the reference flux (0.01 kg m^{-2} yr^{-1} at normalised pressure of 1.0) in the tornado plot (Figure 4). OAT analysis was selected for the screening context because it yields directly interpretable, per-parameter influence measures that practitioners can map onto individual well attributes without requiring ensemble simulation. Its main limitation is that interaction effects between simultaneously varying parameters are not captured; these are addressed through the

Latin Hypercube ensemble in Section 3.4. The computational efficiency of QWellRATE would equally support variance-based global sensitivity methods such as Sobol indices where a site-specific application warrants formal interaction quantification of parameter interactions.

Consistent with the scenario analysis in Section 3.1, Figure 4 demonstrates that cement plug permeability dominates model sensitivity over the two-order-of-magnitude range explored (0.1 to 10 nD, Table 2). Relative to the reference value of 1 nD, a one-order-of-magnitude increase to 10 nD produces an approximately 11-fold flux increase, whereas a one-order-of-magnitude decrease to 0.1 nD produces a comparable reduction. In contrast, other tested parameters (reservoir depth, geothermal gradient, mud permeability, seafloor depth, and plug thickness) elicit a more moderate response, typically producing changes of two-fold or less across their respective perturbation ranges. Mud permeability shows the least sensitivity: increasing it from 10^{-7} to 10^{-3} D substantially changes the non-plug interval resistance but has minimal impact on total flux because the cement plugs already dominate the series resistance of the wellbore system. This illustrates a key principle: in wellbores with intact low-permeability plugs, plug properties control leakage; in unplugged or severely degraded systems, mud and pathway properties become the governing resistance, as demonstrated by the scenario (a) results in Section 3.1. For preliminary site screening and prioritisation, these findings suggest that assessment of existing wellbore integrity databases (completion records, cement bond logs, historical pressure tests, and abandonment plug quality) should take precedence over detailed geological characterisation (Pullen et al., 2025).

Table 2 - Parameters used to define the reference well for sensitivity analysis simulations

Parameter	Reference value	Range tested
Normalized pressure	1.0	N/A
Effective permeability (D)	$1x10^{-5}$	$1x10^{-7} – 1x10^{-3}$
Reservoir depth (mbsf)	1500	500 - 2500
Geothermal gradient (K km^{-1})	30	20 - 40
Seafloor temperature (K)	293.15	N/A
Seafloor depth (mbsl)	100	50 - 150
Number of cement plugs	3	N/A
Plug permeability (D)	$1x10^{-9}$	$1x10^{-10} – 1x10^{-8}$
Plug length (m)	50	10 - 90

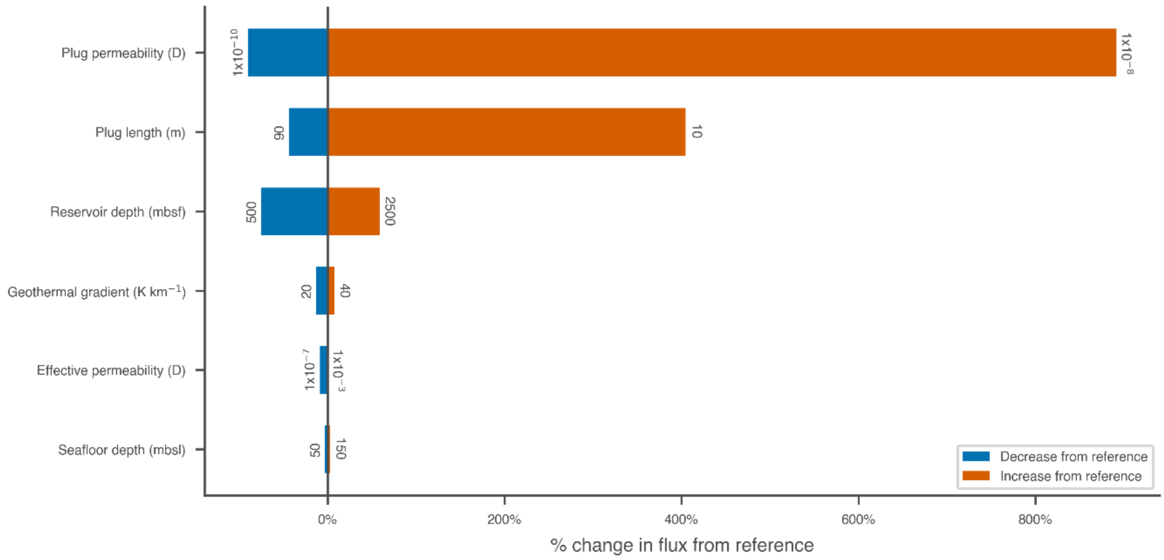

Figure 4: Tornado chart presenting the results of a sensitivity analysis of six input parameters to the wellbore leakage model. Each bar represents a percentage change from the reference condition, which itself is described in Table 2.

The OAT analysis above held pressure constant; Figure 5 extends the analysis to explore how pressure and geological conditions jointly influence leakage flux using scenario (a) (0.01 mD effective mud permeability) to isolate geological effects without confounding from cement plug variability. Figure 5a examines the interaction between normalised pressure and geothermal gradient on leakage flux. Flux increases monotonically with both parameters: across the geothermal gradient range (20–50 K km^{-1}), flux increases by 32–40 % at fixed pressure, while across the normalised pressure range, flux increases by 69–75 % at fixed gradient. The positive effect of geothermal gradient arises because warmer wellbore conditions reduce CO_2 density, lowering the hydrostatic resistance of the CO_2 column, and reduce CO_2 viscosity, increasing fluid mobility. Both effects act in the same direction, producing a monotonic response that is consistent across the pressure range. Figure 5b shows that the seafloor temperature has a similar positive influence on flux, with variation of 48–56 % across the full temperature range at fixed pressure. This is somewhat larger than the geothermal gradient effect and equally consistent across all pressures, reflecting the same physical mechanism operating at the wellbore upper boundary rather than along its length. From a screening perspective, seafloor temperature is therefore at least as influential as geothermal gradient and is more readily available from oceanographic databases.

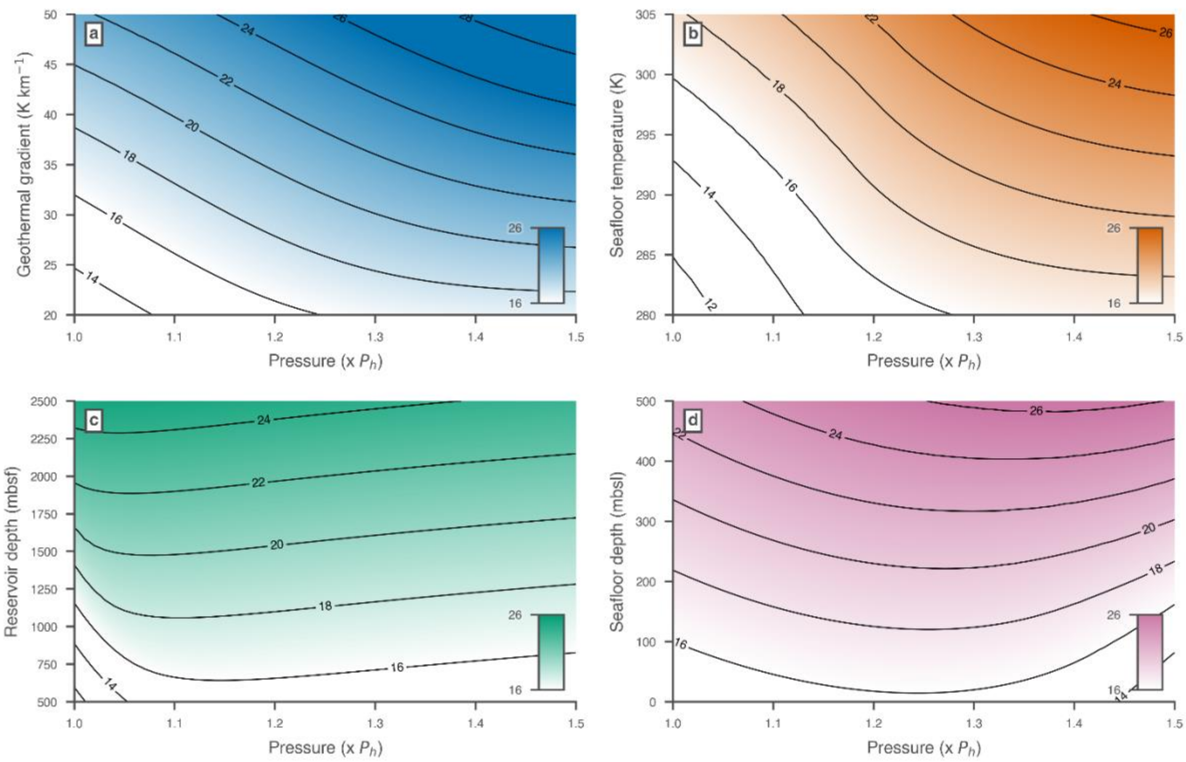

Figure 5: Impact of geological parameters on leakage flux for a wellbore shown in scenario (a) in Figure 2. Both the contours and the colour-shading illustrate flux in kg m^{-2} yr^{-1}. a - Impact of normalized pressure and geothermal gradient, b - Impact of normalized pressure and seafloor temperature, c - Impact of normalized pressure and reservoir depth and d - Impact of normalized pressure and seafloor depth. Where a parameter is not explicitly adjusted, it is set to constant values - Geothermal gradient: 30 K km^{-1}, reservoir depth: 1500 mbsf, seafloor depth: 100 mbsl, seafloor temperature: 293.15 K.

Figure 5c demonstrates that reservoir depth influences flux primarily through its effect on pressure and temperature gradients. Deeper reservoirs create longer migration pathways and higher bottomhole pressures, both of which increase leakage driving force. However, the flux response is sublinear: doubling depth from 1000 to 2000 mbsf increases flux by only ~10 – 25 %. This occurs because deeper pathways traverse more of the P-T regime where CO_2 density is relatively stable, reducing the amplification effect. Figure 5d confirms that seafloor depth exerts the weakest influence among geological parameters. Within the shallow-water range of the Southern North Sea (50–150 m), flux varies by less than 6 % at all pressures, and seafloor depth can be treated as approximately fixed in regional screening for this setting. This occurs because seafloor depth affects only the uppermost 100 m of a 1500+ m pathway, representing a small fraction of total flow resistance. This finding applies to shallow-water environments such as the North Sea; however, in deeper water settings (> 500 m) such as the Gulf of Mexico, water depth would be expected to exert greater influence on leakage flux. Across all four geological parameters, no single parameter alters flux by more than approximately 60% (a factor of 1.6) within realistic ranges, and even their combined worst-case effect remains below a factor of four, confirming that wellbore condition and pressure regime are the primary discriminators at the screening stage (Pan and Oldenburg, 2014; Lu and Connell, 2014).

3.4 Uncertainty analysis

Deterministic sensitivity analysis identifies which parameters govern leakage flux but cannot capture the compounded effect of simultaneous uncertainty across multiple parameters. Real-world wellbores face compounded uncertainties: cement quality varies between plugs, degradation may be spatially heterogeneous, and historical well records often lack precise permeability data. This section addresses that limitation by introducing probabilistic leakage envelopes through Latin Hypercube Sampling (LHS), enabling uncertainty-aware prioritisation across wells and scenarios. We conducted the uncertainty quantification using scenario (c) from Figure 2 as the reference wellbore configuration. Seven parameters were treated as uncertain: effective mud permeability, and the permeability and length of each of the three cement plugs (top, middle, and base). Full parameter distributions are summarised in Table 3. Geothermal gradient and seafloor temperature were held constant, isolating wellbore-specific uncertainties from the geological variability explored in Section 3.3.

Lognormal distributions are assigned to all permeability parameters, as permeability varies multiplicatively across orders of magnitude in subsurface systems (Checkai et al., 2013). The standard deviations (σ = 3.0 for mud permeability, σ = 4.0 for plug permeability) reflect 6-12 orders of magnitude spanned by effective cement permeability from intact to severely degraded states, encompassing the full range of integrity conditions expected across a legacy well population (Torsæter et al., 2024). Plug length is assigned a normal distribution with mean 30 m and standard deviation 20 m, reflecting the regulatory evolution from approximately 20 m (pre-2004) to 50 m (post-2004) requirements and accounting for placement uncertainty (Torsæter et al., 2024).

We generated 10,000 parameter realizations using LHS and calculated leakage flux for each across normalized pressures from 1.0 (hydrostatic) to 1.5 (50% overpressure). Figure 6 presents the full ensemble, with individual realisations shown as grey points, the median flux (P50) as a solid blue line, and ±1 standard deviation as the shaded region. Leakage flux spans nearly five orders of magnitude (10^{-1} to 10^{4} kg m^{-2} yr^{-1}) across the ensemble, substantially exceeding the two-fold parameter sensitivities observed in Section 3.3. This multiplicative amplification arises from simultaneous degradation across multiple plugs combined with elevated mud permeability and cannot be predicted from single-parameter analysis alone. Percentile estimates are provided in Table 4. All percentiles (P10, P50, P90) increase monotonically with reservoir pressure; P90 values are approximately two to three times higher than the corresponding P50 values and approximately ten times higher than P10, indicating a positively skewed distribution in which tail-risk realisations substantially exceed the median.

The P50 flux magnitudes reported here (480 - 700 kg m^{-2} yr^{-1}) substantially exceed those in Section 3.1 (0.02–24 kg m^{-2} yr^{-1} for scenario (c)). This difference arises directly from the parameter distributions: the lognormal distribution for plug permeability assigns a mean of 100 nD (Table 3), two orders of magnitude above the 1 nD reference case, while plug lengths are distributed around a mean of 30 m rather than the 50 m reference. The lognormal distributions for plug permeability and mud permeability (Table 3) capture degradation scenarios beyond the reference cases in Section 3.1. The P50 therefore represents the expected outcome across a realistic population of legacy wells where some degree of plug degradation is common, not a worst-case estimate. These magnitudes are consistent with pre-oxidation CH_4 flux estimates from field analogues (Appendix B), which account for microbial oxidation losses and therefore represent total subsurface leakage rather than surface emissions alone, providing empirical support for the physical plausibility of the ensemble results. The P90 values, representing the upper decile of the parameter distribution, capture tail-risk scenarios arising from simultaneous degradation across multiple plugs and are necessary for screening-level decision support where false negatives carry the greatest consequence.

The percentile estimates are conditioned on the parameter distributions in Table 3, which represent generic field variability rather than site-specific characterisation. For individual storage projects, distribution parameters should be refined using site well data, well logs, and cement bond quality assessments, and the analysis repeated to derive project-specific risk estimates. The computational efficiency of QWellRATE (10,000 realisations in under 3 hours on an Apple MacBook Pro with M4 chip) enables such site-specific probabilistic assessment. The five-order-of-magnitude ensemble range substantially exceeds the single-parameter sensitivities identified in Section 3.3, confirming that multiplicative interaction between degraded cement and elevated mud permeability is the primary driver of tail-risk outcomes, and motivating ensemble approaches for any legacy well population where barrier integrity is uncertain.

Table 3 - Parameters used to define the reference well for uncertainty analysis.

Parameter	Mean value	Distribution	Notes
Effective mud permeability (D)	1×10^{-5}	Lognormal (σ = 3.0)	Truncated: 10^{-8} to 10^{-2} D
Plug 1 Permeability (D)	1×10^{-7}	Lognormal (σ = 4.0)	Truncated: 10^{-12} to 1 D
Plug 2 Permeability (D)	1×10^{-7}	Lognormal (σ = 4.0)	Truncated: 10^{-12} to 1 D
Plug 3 Permeability (D)	1×10^{-7}	Lognormal (σ = 4.0)	Truncated: 10^{-12} to 1 D
Plug 1 Length (m)	30	Normal (σ = 20 m)	Truncated: 1 to 60 m
Plug 2 Length (m)	30	Normal (σ = 20 m)	Truncated: 1 to 60 m
Plug 3 Length (m)	30	Normal (σ = 20 m)	Truncated: 1 to 60 m
Geothermal gradient (K km^{-1})	30		Constant
Seafloor temperature (K)	293.15		Constant

Note: Permeabilities use lognormal distributions with σ representing standard deviation of log_{10}(permeability) and plug lengths use normal distributions, both truncated to the mentioned ranges to prevent unrealistic values.

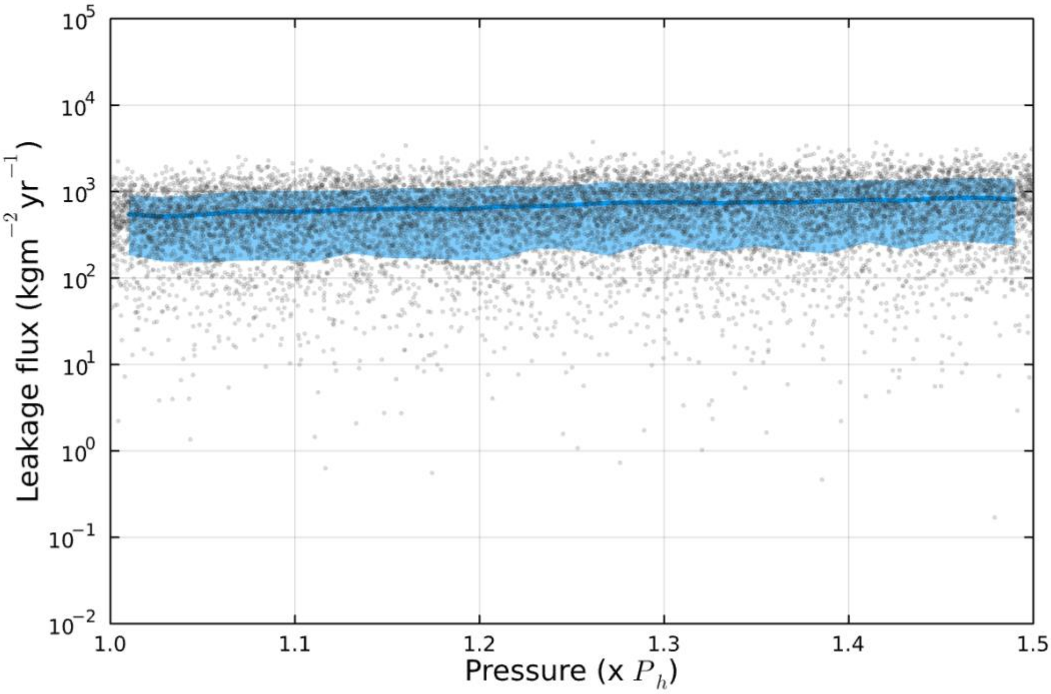

Figure 6: Uncertainty quantification of CO_2 leakage flux as a function of normalized reservoir pressure for wellbore scenario (c) from Figure 2. Each gray point represents an individual simulation realization; the solid blue line is the median predicted flux, and the blue shaded region spans ±1 standard deviation. Parameter distributions in Table 3.

Table 4 - Percentile flux estimates from Latin Hypercube Sampling analysis

Normalized Pressure	P10 (kg m^{-2} yr^{-1})	P50 (kg m^{-2} yr^{-1})	P90 (kg m^{-2} yr^{-1})
1.0 – 1.1	114.34	482.78	1103.39
1.1 – 1.2	119.74	531.17	1227.97
1.2 – 1.3	134.35	604.24	1397.16
1.3 – 1.4	144.63	653.59	1491.20
1.4 - 1.5	173.64	704.06	1618.69

3.5 Mapping potential leakage fluxes in the UK Southern North Sea

Recent regional-scale assessments have highlighted that pressure perturbations associated with CO_2 injection in mature basins extend well beyond the plume footprint and inevitably intersect legacy wells, even where injector siting avoids direct plume–well contact (Smith et al., 2026). While such studies motivate the need for basin-scale planning and coordination, the present work addresses the complementary question of what those interactions imply at the wellbore scale. We apply QWellRATE to the Southern North Sea to illustrate its capability for regional spatial screening, using the

Leman Sandstone Formation as a representative CO_2 storage target in the region (Underhill et al., 2023). We emphasise that this analysis uses assumed wellbore properties (Table 5) and is intended to illustrate the tool's spatial screening capability rather than provide validated predictions for actual wells. Regularly gridded datasets of reservoir and seafloor depth were obtained from publicly available sources (GEBCO Compilation Group, 2024; NSTA, 2025) and resampled to a 2500 m × 2500 m grid covering approximately 2500 km^2 near the Leman and Indefatigable gas fields, resulting in 400 grid cells. A geothermal gradient of 25 K km^{-1} and seafloor temperature of 293.15 K were assumed, following Hollinsworth et al. (2022). Each wellbore was modelled as scenario (c): three 50 m cement plugs placed at 20 %, 50 %, and 80 % of reservoir depth. Table 5 defines the four scenarios evaluating the impact of pressure regime and plug permeability on spatial leakage patterns.

Table 5: Outline of the four scenarios used to investigate the role of pressure and plug permeability on leakage rates in a region of the Southern North Sea. The lettering (c)-(f) refers to panels in Figure 7.

Scenario	Normalized Pressure	Permeability of plugs
(c) Base case (maintained plugs)	1.0	1 nD
(d) Overpressured, maintained plugs	1.5	1 nD
(e) Hydrostatic, degraded plugs	1.0	1 μD
(f) Overpressured, degraded plugs	1.5	1 μD

Figure 7 maps leakage flux across the study area for all four scenarios. Modelled fluxes span approximately three orders of magnitude from 10^{-2} kg m^{-2} yr^{-1} under base case conditions (maintained plugs, hydrostatic pressure; Figure 7c) to approximately 15 kg m^{-2} yr^{-1} under severe conditions (degraded plugs, overpressured; Figure 7f). Plug degradation (permeability increase from 1 nD to 1 μD) produces the largest spatial impact, with increase of 200-300x across the region. At the shallower reference location X1 (~1900 mbsf), base-case flux of approximately 10^{-2} kg m^{-2} yr^{-1} increases to approximately 1 kg m^{-2} yr^{-1} under plug degradation alone. At the deeper location X2 (~2800 mbsf), fluxes increase from approximately 5 x 10^{-2} kg m^{-2} yr^{-1} to approximately 15 kg m^{-2} yr^{-1} under combined overpressure and plug degradation. Overpressure alone, with maintained plug integrity, produces 70–100 % flux increases across the region, compared to 50–70 % when plugs are already degraded, indicating a non-linear interaction between pressure regime and plug condition. North-eastern locations systematically exhibit elevated leakage across all scenarios, highlighting priority areas that may require targeted monitoring.

Base-case fluxes across the study area range from approximately 0.02 – 0.04 kg m^{-2} yr^{-1}, consistent with low leakage potential for the Leman Sandstone under intact barrier and hydrostatic conditions. Under degraded plug conditions, a three-order-of-magnitude increase in plug permeability (1 nD to 1 μD) produces fluxes of up to approximately 15.1 kg m^{-2} yr^{-1}, underscoring the sensitivity of regional leakage potential to barrier integrity.

The spatial heterogeneity and non-linear interaction between pressure regime and plug condition across scenarios demonstrate the value of probabilistic spatial screening over single deterministic assessment.

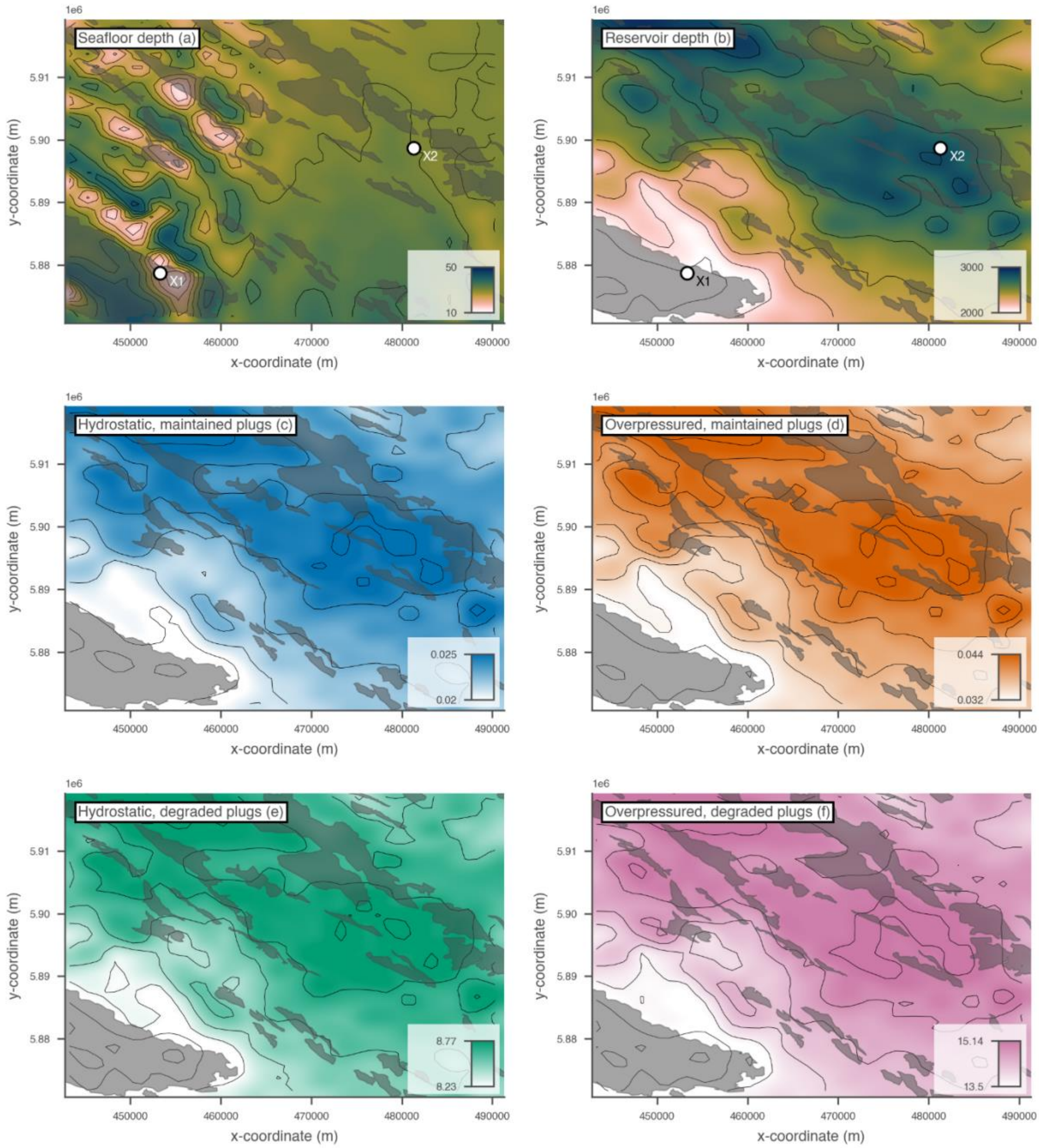

Figure 7: Maps of leakage flux for four scenarios, generated using gridded datasets of seafloor depth (a) and reservoir depth (b). Panels (c) to (f) illustrate modelling results for four scenarios described in Table 5. Note that each panel is illustrated using different scaling. X1 and X2 refer to two locations of interest as described in the text. The moderately opaque, gray polygons are existing gas fields in the area.

We stress that this exercise illustrates a possible regional deployment of QWellRATE rather than a set of results from which validated conclusions about leakage fluxes in the Southern North Sea could be drawn. Several limitations would need to be addressed before results could inform site-specific decisions. First, wellbore properties (Table 5) are assumed uniform across all grid cells, whereas actual conditions vary between wells depending on construction era, operator practices, and abandonment procedures. Second, we model a single representative wellbore per grid cell, whereas actual storage projects must account for multiple wells within developed fields. Third, actual pressure distributions during injection, which would be determined by reservoir simulation considering injection rates, formation properties, and hydraulic connectivity, are not incorporated.

3.6 Discussion

The analyses in Sections 3.1–3.5 establish a consistent hierarchy of controls on CO_2 leakage flux from legacy wellbores across multiple analytical frameworks. Cement plug permeability is the primary determinant at all scales of analysis: the scenario comparison (Section 3.1), OAT sensitivity (Section 3.3), and LHS ensemble (Section 3.4) all confirm that plug permeability variation produces orders-of-magnitude flux changes, whereas all four geological parameters combined span less than a factor of three across realistic parameter ranges (Section 3.3). Normalised reservoir overpressure is the second-order control, with a 50 % increase in normalised pressure producing a 61–75 % flux increase across all geological configurations examined, reflecting CO_2 thermophysical non-linearities that simplified isothermal formulations cannot capture. These findings are corroborated by the benchmarking in Section 3.2, which confirms that the flux envelope produced by QWellRATE across barrier-integrity states is empirically plausible against independent field analogue data.

A cross-cutting result from Sections 3.1 and 3.4 is the non-linear response of multi-barrier systems to progressive degradation. Single-plug or dual-plug degradation causes less than a four-fold flux increase as the remaining intact plugs absorb the additional driving force; simultaneous degradation of all three barriers produces a 500-fold increase, approaching the flux of an unplugged well. The LHS ensemble confirms this non-linearity at the population level: the five-order-of-magnitude ensemble range far exceeds the two-fold single-parameter sensitivities observed in the OAT analysis, driven by multiplicative interactions between degraded plug permeability, shortened plug length, and elevated mud permeability. The transition from manageable to critical leakage risk is therefore sudden rather than gradual and depends on whether redundant barriers remain intact. This result motivates monitoring strategies capable of detecting early-stage degradation before multiple barriers fail simultaneously, rather than strategies calibrated to detect post-failure surface emissions.

Across Sections 3.1, 3.3, and 3.4, the following parameter thresholds consistently distinguish higher-risk from lower-risk configurations and provide a practical basis for screening-level prioritisation. Wells with fewer than two cement plugs, plug lengths below approximately 50 m, or estimated plug permeabilities exceeding approximately 100 nD across multiple barriers should be assigned higher priority for follow-up assessment. The association of these characteristics with well vintage provides a first-pass screening entry point requiring only abandonment-era information: pre-standardisation wells (pre-1990) lack formal plug placement and correspond to scenario (a) configurations with the highest leakage potential; transitional-era wells (1990–2004) carry one to two plugs but may fall below the 50 m length threshold; modern wells (post-2004) are most likely to satisfy the multi-plug, minimum-50 m configuration of scenario (c) with the lowest baseline risk. Where P90 ensemble flux exceeds regulatory thresholds even if P50 remains acceptable (Section 3.4), targeted integrity verification should be considered regardless of vintage. The regional demonstration in Section 3.5 illustrates how these criteria can be applied spatially to identify priority clusters before well-specific integrity data are available.

It is useful to situate QWellRATE within the landscape of established wellbore leakage frameworks. The wellbore components of NRAP-Open-IAM (Vasylkivska et al., 2021), including the multisegmented wellbore model based on Nordbotten et al. (2009) and reduced-order models trained on full-physics simulations (Jordan et al., 2015; Harp et al., 2016; Baek et al., 2023), are designed for integrated whole-system risk assessment of characterised storage sites. These components adopt isothermal flow formulations, require transient pressure and saturation boundary conditions supplied by a coupled reservoir model (Baek et al., 2021), and were developed primarily for deep saline aquifer scenarios in the United States. QWellRATE addresses a different stage of the assessment workflow: it operates on readily available well and reservoir inputs without requiring coupled reservoir simulation, evaluates depth-dependent CO_2 thermophysical properties that isothermal formulations neglect, and is parameterised for the legacy-well configurations characteristic of mature petroleum provinces such as the UK North Sea. The two approaches are complementary rather than competing: QWellRATE provides inventory-scale triage identifying which wells warrant the site-specific characterisation and coupled reservoir modelling that frameworks such as NRAP-Open-IAM then support (Pullen et al., 2025; Smith et al., 2026). The computational efficiency demonstrated in Sections 3.4 and 3.5 makes this triage step practical at the scale of mature petroleum provinces hosting thousands of legacy wells.

4. Conclusions

This study addresses a critical gap in legacy well screening for CO_2 storage: the need for rapid, physics-based flux estimation across large well populations where integrity data are uncertain. We present QWellRATE, a simplified steady-state screening tool that estimates upper-bound CO_2 leakage fluxes along legacy wellbore pathways using the Span–Wagner equation of state for depth-dependent thermophysical properties and an equivalent Darcy continuum representation of the leakage pathway. The model operates on readily available well and reservoir inputs and produces flux magnitudes consistent with analogue field observations across well configurations ranging from intact multi-plug systems to unplugged pathways.

Cement plug permeability is the primary control on leakage flux at the screening stage. Two intact cement plugs reduce flux by approximately 760-fold relative to an unplugged well; plug lengths beyond 50 m offer diminishing additional resistance, with less than a two-fold further reduction from 50 to 90 m. Progressive barrier degradation follows a strongly non-linear pattern: single-plug or dual-plug degradation increases flux by less than four-fold as intact barriers absorb the additional driving force, whereas simultaneous degradation of all three plugs produces an approximately 500-fold increase. Geological parameters collectively span less than a factor of three across realistic North Sea ranges, confirming that abandonment quality outweighs geological variability for containment risk at the screening stage. Uncertainty quantification via Latin Hypercube Sampling yields a five-order-of-magnitude flux range (10^{-1} to 10^{4} kg m^{-2} yr^{-1}), confirming that multiplicative interactions between degraded cement and elevated mud permeability drive tail-risk outcomes far beyond single-parameter sensitivities.

These findings support prioritisation by well vintage, pre-standardisation wells with no formal plug placement carry the highest baseline risk, modern multi-plug wells the lowest, and by parameter thresholds: fewer than two plugs, plug lengths below 50 m, or plug permeabilities exceeding 100 nD across multiple barriers warrant elevated priority for follow-up assessment. Regional demonstration in the Southern North Sea completes 1600 spatial realisations in under one hour, with plug permeability increases from 1 nD to 1 μD producing 200–300x flux increases across the region. The computational efficiency of QWellRATE (10,000 realisations in under 3 hours) enables rapid inventory-scale screening to identify high-risk candidates for follow-up with high-fidelity multiphase simulators, complementing established frameworks such as NRAP-Open-IAM that operate at a later, data-rich stage of site assessment. Future extensions could incorporate time-dependent barrier degradation and multiphase flow during CO_2 breakthrough; the current formulation provides rapid upper-bound flux estimates appropriate for the screening stage where well integrity data are sparse.

Appendix A

This appendix verifies the numerical implementation of QWellRATE against an independent full-physics simulator for an identical 1D non-isothermal flow problem; benchmarking against field-analogue flux observations is presented separately in Section 3.2 and Appendix B. QWellRATE results agree well with the CMG-GEM simulator (compositional EOS reservoir simulator (CMG, 2015) as shown in Figure A1 for parameters in Table A1. We compare numerical solution for 1D CO_2 vertical flow with variable temperature profile using identical pathway properties. The CMG-GEM pressure profile reached steady state after 100 days. Minor differences between pressure profiles result from different fluid property models. The fluid properties were estimated using Peng-Robinson EOS (Peng & Robinson, 1976), and the viscosity was calculated with a corresponding states model in CMG (Pedersen et al., 1984). The model presented here uses the Span - Wagner EOS (Span & Wagner, 2003a, 2003b), and viscosity is calculated with a corresponding states model (Vesovic et al., 1990; Fenghour et al., 1998).

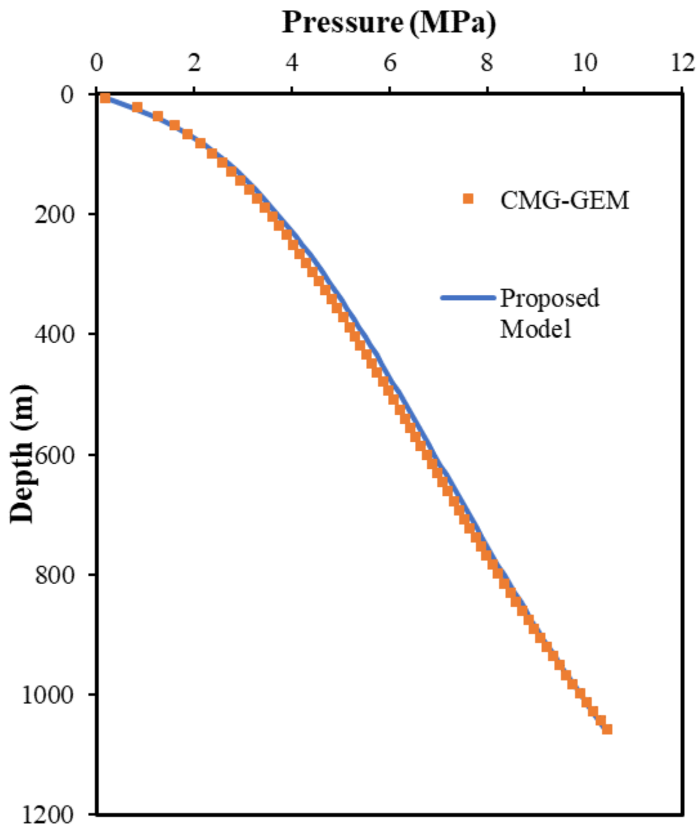

Figure A1: Pressure profiles versus depth for CMG-GEM reservoir simulator and QWellRATE. Results show good agreement.

Table A1: Input parameters for model verification

Parameters	**CMG**	**Model**
Number of grid blocks (nx,ny,nz)	(1,1,70)	(1,1,70)
Dimensions of grid blocks (m), Δx	0.10	0.10
Dimensions of grid blocks (m), Δy	10.00	10.00
Dimensions of grid blocks (m), Δz	15.25	15.25
Length of the pathway (m)	1067.00	1067.00
Pathway permeability (D), k	1.00	1.00
Pathway porosity, ϕ	0.30	0.30
Initial Conditions		
Surface temperature (K), Tsf	289.15	289.15
Geothermal gradient (K/km), GG	0.03	0.03
Residual water saturation	0.20	0.20
Initial water saturation	0.20	0.20
Initial gas saturation	0.80	0.80
Boundary Conditions		

Pressure at the base, MPa	10.4983	10.4983
Pressure at the top, MPa	0.1552	0.1552
Relative permeability constants for corey curve		
Gas phase end point	0.70	0.70
Gas phase exponent	4.00	4.00

Appendix B

This section details the field analogue flux processing used in section 3.2. Mapped excess (above-background) CH_4 and CO_2 fluxes from Cahill et al. (2023, 2025) were converted to total molar fluxes (μmol s^{-1}). Assuming that the measured excess CO_2 originates entirely from the oxidation of leaked CH_4 within the soil column, the total (pre-oxidation) CH_4 leakage rate can be expressed as:

$$n_{CH_4\_pre} = n_{CH_4\_ex} + n_{CO_2\_ex} \tag{B1}$$

Where $n_{CH_4\_pre}$ is the total CH_4 released from the well before oxidation (mol s^{-1}), $n_{CH_4\_ex}$ is the measured excess CH_4 flux at the surface (mol s^{-1}), and $n_{CO_2\_ex}$ is the excess CO_2 flux attributed to complete CH_4 oxidation (mol s^{-1}). Totals were converted to kg yr^{-1} using the molar mass of CH_4 (16.04 g mol^{-1}) and normalised by the mapped footprint area to yield kg m^{-2} yr^{-1}. The post-oxidation (surface-emitted) flux reported in the main text uses $n_{CH_4\_ex}$ only and represents a measurement-based lower bound. Applying the findings to the Cahill et al. (2025) Wellsite J data, the calculations show a pre-oxidation methane emission rate of approximately 466 kg CH_4 yr^{-1} (or ~ 13 kg m^{-2} yr^{-1}), which was reduced post-oxidation to roughly 28 kg CH_4 yr^{-1} (or ~ 1 kg m^{-2} yr^{-1}), implying a CH_4 oxidation efficiency of approximately 94 %. Flux ranges from Riddick et al. (2020) (< 1 mg h^{-1} – 80 g h^{-1} per well) and Forde et al. (2019) (0.017 – 180 μmol m^{-2} s^{-1} ~ 0.009 – 91 kg m^{-2} yr^{-1}) represent post-oxidation surface emissions and provide contextual variability bounds.

Acknowledgments

This work was supported by the Flexible Funding 2024 grant for project ''Development of a Quantitative Legacy Wellbore Risk Assessment Tool for Enabling Storage Projects (QWellRATE)' from UK Carbon Capture and Storage Research Centre (UKCCSRC), which is funded by the Engineering and Physical Sciences Research Council (EPSRC) as part of the UK Research and Innovation (UKRI) Energy Programme.

CRediT Statement

Hariharan Ramachandran: Conceptualization, Methodology, Software, Validation, Formal analysis, Investigation, Writing - Original Draft, Visualization **Iain de-Jonge Anderson:** Formal analysis, Investigation, Resources, Data curation, Visualization, Writing - Review & Editing **Benjamin Pullen:** Formal Analysis, Investigation, Writing -

Review & Editing **Aaron Cahill:** Conceptualization, Methodology, Formal analysis, Investigation, Writing - Review & Editing, Supervision, Project administration, Funding acquisition

Data Availability Statement

The QWellRATE model is available on Zenodo (DOI: 10.5281/zenodo.17485764). All publicly available datasets used in this study are cited in the manuscript and accessible through the references provided.

AI statement

During the preparation of this work the author(s) used Claude in order to improve the readability. After using this tool/service, the author(s) reviewed and edited the content as needed and take(s) full responsibility for the content of the published article.

References

Arbad, N., Watson, M., Emadi, H., Eyitayo, S., & Leggett, S. (2024). Strategic qualitative risk assessment of thousands of legacy wells within the area of review (Aor) of a potential co2 storage site. *Minerals*, *14*(4), 383. https://doi.org/10.3390/min14040383

Arild, Ø., Lohne, H. P., Nielsen, M., Moeinikia, F., Selvik, J. T., Abrahamsen, E. B., Ford, E. P., & Mansouri Majoumerd, M. (2018). Permanent p&a design—What is good enough? *SPE Annual Technical Conference and Exhibition*, D021S013R004. https://doi.org/10.2118/191414-MS

Arzanfudi, M. M., & Al-Khoury, R. (2017). Thermo-hydrodynamic-mechanical multiphase flow model for CO_2 sequestration in fracturing porous media. *International Journal for Numerical Methods in Fluids*, *84*(11), 635–674. https://doi.org/10.1002/fld.4364

Bachu, S., & Bennion, D. B. (2009). Experimental assessment of brine and/or CO2 leakage through well cements at reservoir conditions. *International Journal of Greenhouse Gas Control*, *3*(4), 494-501. https://doi.org/10.1016/j.ijggc.2008.11.002

Baek, S., Bacon, D. H., & Huerta, N. J. (2023). Enabling site-specific well leakage risk estimation during geologic carbon sequestration using a modular deep-learning-based wellbore leakage model. *International Journal of Greenhouse Gas Control*, *126*, 103903. https://doi.org/10.1016/j.ijggc.2023.103903

Baek, S., Hibbard, L., Mitchell, N., Appriou, D., Dilmore, R., & Mamud, M. (2025). Deep-learning-enhanced assessment of wellbore barrier effectiveness in geologic storage systems with intermediate aquifers. *International Journal of Greenhouse Gas Control*, *147*, 104487. https://doi.org/10.1016/j.ijggc.2025.104487

Bai, M., Zhang, Z., & Fu, X. (2016). A review on well integrity issues for CO 2 geological storage and enhanced gas recovery. *Renewable and Sustainable Energy Reviews*, *59*, 920–926. https://doi.org/10.1016/j.rser.2016.01.043

Bezanson, J., Edelman, A., Karpinski, S., & Shah, V. B. (2017). Julia: A fresh approach to numerical computing. *SIAM Review*, *59*(1), 65–98. https://doi.org/10.1137/141000671

Blackford, J., Stahl, H., Bull, J. M., Bergès, B. J. P., Cevatoglu, M., Lichtschlag, A., Connelly, D., James, R. H., Kita, J., Long, D., Naylor, M., Shitashima, K., Smith, D., Taylor, P., Wright, I., Akhurst, M., Chen, B., Gernon, T. M., Hauton, C., ... Widdicombe, S. (2014). Detection and impacts of leakage from sub-seafloor deep geological carbon dioxide storage. *Nature Climate Change*, *4*(11), 1011–1016. https://doi.org/10.1038/nclimate2381

Böttcher, N., Taron, J., Kolditz, O., Park, C.-H., & Liedl, R. (2012). Evaluation of thermal equations of state for CO2 in numerical simulations. *Environmental Earth Sciences*, *67*(2), 481–495. https://doi.org/10.1007/s12665-012-1704-1

Bowman, L. (2023). *Abandoned oil and gas wells in Western Canada: methane measurements and emission estimates*. McGill University (Canada).

Bump, A. P., & Hovorka, S. D. (2023). Fetch-trap Pairs: Exploring definition of carbon storage prospects to increase capacity and flexibility in areas with competing uses. *International Journal of Greenhouse Gas Control*, *122*, 103817. https://doi.org/10.1016/j.ijggc.2022.103817

Cahill, A. G., Joukar, M., Sefat, M., & Van Geloven, C. (2023). Evaluating methane emissions from decommissioned unconventional petroleum wells in british columbia, canada. *Geophysical Research Letters*, *50*(24), e2023GL106496. https://doi.org/10.1029/2023GL106496

Cai, Y., Lei, H., Li, X., Feng, G., Cui, Y., & Bai, B. (2022). Modeling of possible CO2 leakage with phase transition in wellbore-reservoir system based on the Ordos CCS project, China. *International Journal of Greenhouse Gas Control*, *114*, 103578. https://doi.org/10.1016/j.ijggc.2021.103578

Carey, J. W., Svec, R., Grigg, R., Zhang, J., & Crow, W. (2010). Experimental investigation of wellbore integrity and CO2–brine flow along the casing–cement microannulus. *International Journal of Greenhouse Gas Control*, *4*(2), 272-282. https://doi.org/10.1016/j.ijggc.2009.09.018

Celia, M. A., Nordbotten, J. M., Court, B., Dobossy, M., & Bachu, S. (2011). Field-scale application of a semi-analytical model for estimation of CO2 and brine leakage along old wells. *International Journal of Greenhouse Gas Control*, *5*(2), 257–269. https://doi.org/10.1016/j.ijggc.2010.10.005

Checkai, D., Bryant, S., & Tao, Q. (2013). Towards a frequency distribution of effective permeabilities of leaky wellbores. *Energy Procedia*, *37*, 5653–5660. https://doi.org/10.1016/j.egypro.2013.06.487

Chukwuemeka, A. O., Oluyemi, G., Mohammed, A. I., & Njuguna, J. (2023). Plug and abandonment of oil and gas wells – A comprehensive review of regulations, practices, and related impact of materials selection. *Geoenergy Science and Engineering*, *226*, 211718. https://doi.org/10.1016/j.geoen.2023.211718

CMG. 2015. CMG GEM User's Guide. Calgary, Alberta, Canada: Computer Modelling Group Ltd.

Davies, R. J., Almond, S., Ward, R. S., Jackson, R. B., Adams, C., Worrall, F., Herringshaw, L. G., Gluyas, J. G., & Whitehead, M. A. (2014). Oil and gas wells and their integrity: Implications for shale and unconventional resource exploitation.

Marine and Petroleum Geology, *56*, 239–254. https://doi.org/10.1016/j.marpetgeo.2014.03.001

Ebigbo, A., Class, H., & Helmig, R. (2007). CO2 leakage through an abandoned well: Problem-oriented benchmarks. *Computational Geosciences*, *11*(2), 103–115. https://doi.org/10.1007/s10596-006-9033-7

Fenghour, A., Wakeham, W. A., & Vesovic, V. (1998). The viscosity of carbon dioxide. *Journal of Physical and Chemical Reference Data*, *27*(1), 31–44. https://doi.org/10.1063/1.556013

Forde, O. N., Cahill, A. G., Beckie, R. D., & Mayer, K. U. (2019). Barometric-pumping controls fugitive gas emissions from a vadose zone natural gas release. *Scientific Reports*, *9*(1), 14080. https://doi.org/10.1038/s41598-019-50426-3

Gan, M., Nguyen, M. C., Zhang, L., Wei, N., Li, J., Lei, H., Wang, Y., Li, X., & Stauffer, P. H. (2021). Impact of reservoir parameters and wellbore permeability uncertainties on CO2 and brine leakage potential at the Shenhua CO2 Storage Site, China. *International Journal of Greenhouse Gas Control*, *111*, 103443. https://doi.org/10.1016/j.ijggc.2021.103443

Gasda, S. E., Bachu, S., & Celia, M. A. (2004). Spatial characterization of the location of potentially leaky wells penetrating a deep saline aquifer in a mature sedimentary basin. *Environmental Geology*, *46*(6–7), 707–720. https://doi.org/10.1007/s00254-004-1073-5

GEBCO Bathymetric Compilation Group 2024. (2024). The GEBCO_2024 Grid - a continuous terrain model of the global oceans and land. https://doi.org/10.5285/1c44ce99-0a0d-5f4f-e063-7086abc0ea0f

Harooni, A. B., Sedeh, M. S., Farzaneh, S. A., & Fahimpour, J. (2025). Experimental investigation of gas permeability and flow behaviour in wellbore cements. *International Journal of Greenhouse Gas Control*, *147*, 104489. https://doi.org/10.1016/j.ijggc.2025.104489

Harp, D. R., Pawar, R., & Gable, C. W. (2014). Numerical modeling of cemented wellbore leakage from storage reservoirs with secondary capture due to thief zones. Energy Procedia, 63, 3532–3543. https://doi.org/10.1016/j.egypro.2014.11.382

Harp, D. R., Pawar, R., Carey, J. W., & Gable, C. W. (2016). Reduced order models of transient CO2 and brine leakage along abandoned wellbores from geologic carbon sequestration reservoirs. *International Journal of Greenhouse Gas Control*, *45*, 150–162. https://doi.org/10.1016/j.ijggc.2015.12.001

Hollinsworth, A. D., I. de Jonge-Anderson, J. R. Underhill, and R. J. Jamieson. "Geological Evaluation of Suprasalt Carbon Storage Opportunities in the Silverpit Basin, United Kingdom Southern North Sea." AAPG Bulletin 106, no. 9 (2022): 1791-825. https://doi.org/10.1306/03232221119.

Huerta, N. J., Checkai, D. A., & Bryant, S. L. (2009). Utilizing sustained casing pressure analog to provide parameters to study co2 leakage rates along a wellbore. *SPE International Conference on CO2 Capture, Storage, and Utilization*, SPE-126700-MS. https://doi.org/10.2118/126700-MS

Humez, P., Audigane, P., Lions, J., Chiaberge, C., & Bellenfant, G. (2011). Modeling of co2 leakage up through an abandoned well from deep saline aquifer to shallow fresh groundwaters. *Transport in Porous Media*, *90*(1), 153–181. https://doi.org/10.1007/s11242-011-9801-2

Iyer, J., Walsh, S. D. C., Hao, Y., & Carroll, S. A. (2018). Assessment of two-phase flow on the chemical alteration and sealing of leakage pathways in cemented wellbores. *International Journal of Greenhouse Gas Control*, *69*, 72–80. https://doi.org/10.1016/j.ijggc.2017.12.001

Johnson, C., Sefat, M. H., & Davies, D. (2021). Developing a well-centric flow model—The first step in a risk-based approach to oil and gas well decommissioning. *Journal of Petroleum Science and Engineering*, *204*, 108651. https://doi.org/10.1016/j.petrol.2021.108651

Jordan, A. B., Stauffer, P. H., Harp, D., Carey, J. W., & Pawar, R. J. (2015). A response surface model to predict CO2 and brine leakage along cemented wellbores. *International Journal of Greenhouse Gas Control*, *33*, 27–39. https://doi.org/10.1016/j.ijggc.2014.12.002

Kaiser, M. J., & Dodson, R. D. (2008). Trends in plug and abandonment cost in the Gulf of Mexico, 2002? 2007. *International Journal of Oil, Gas and Coal Technology*, *1*(1-2), 24-45.

Kang, M., Kanno, C. M., Reid, M. C., Zhang, X., Mauzerall, D. L., Celia, M. A., Chen, Y., & Onstott, T. C. (2014). Direct measurements of methane emissions from abandoned oil and gas wells in Pennsylvania. *Proceedings of the National Academy of Sciences*, *111*(51), 18173–18177. https://doi.org/10.1073/pnas.1408315111

Keating, E. H., Harp, D. H., Dai, Z., & Pawar, R. J. (2016). Reduced order models for assessing CO2 impacts in shallow unconfined aquifers. *International Journal of Greenhouse Gas Control*, *46*, 187–196. https://doi.org/10.1016/j.ijggc.2016.01.008

Khalifeh, M., & Saasen, A. (2020). *Introduction to Permanent Plug and Abandonment of Wells* (Vol. 12). Springer International Publishing. https://doi.org/10.1007/978-3-030-39970-2

Kim, T. W., Li, Y., Kohli, A. H., & Kovscek, A. R. (2025). Assessment of CO2 leakage through existing wells and faults for a prospective storage site in the Southern San Joaquin Basin, California. *International Journal of Greenhouse Gas Control*, *144*, 104381. https://doi.org/10.1016/j.ijggc.2025.104381

King, G. E., & King, D. E. (2013). Environmental risk arising from well-construction failure—differences between barrier and well failure, and estimates of failure frequency across common well types, locations, and well age. *SPE Production & Operations*, *28*(04), 323-344.

King, G. E., & Valencia, R. L. (2014). Environmental risk and well integrity of plugged and abandoned wells. *SPE Annual Technical Conference and Exhibition*, SPE-170949-MS. https://doi.org/10.2118/170949-MS

Kiran, R., Teodoriu, C., Dadmohammadi, Y., Nygaard, R., Wood, D., Mokhtari, M., & Salehi, S. (2017). Identification and evaluation of well integrity and causes of failure of well integrity barriers (A review). *Journal of Natural Gas Science and Engineering*, *45*, 511–526. https://doi.org/10.1016/j.jngse.2017.05.009

Kopp, A., Binning, P. J., Johannsen, K., Helmig, R., & Class, H. (2010). A contribution to risk analysis for leakage through abandoned wells in geological CO2 storage. *Advances in Water Resources*, *33*(8), 867–879. https://doi.org/10.1016/j.advwatres.2010.05.00

Krevor, S., De Coninck, H., Gasda, S. E., Ghaleigh, N. S., De Gooyert, V., Hajibeygi, H., Juanes, R., Neufeld, J., Roberts, J. J., & Swennenhuis, F. (2023). Subsurface carbon dioxide and hydrogen storage for a sustainable energy future. *Nature Reviews Earth & Environment*, *4*(2), 102–118. https://doi.org/10.1038/s43017-022-00376-8

Lackey, G., Rajaram, H., Bolander, J., Sherwood, O. A., Ryan, J. N., Shih, C. Y., Bromhal, G. S., & Dilmore, R. M. (2021). Public data from three US states provide new insights into well integrity. *Proceedings of the National Academy of Sciences*, *118*(14), e2013894118. https://doi.org/10.1073/pnas.2013894118

Lackey, G., Vasylkivska, V. S., Huerta, N. J., King, S., & Dilmore, R. M. (2019). Managing well leakage risks at a geologic carbon storage site with many wells. *International Journal of Greenhouse Gas Control*, *88*, 182–194. https://doi.org/10.1016/j.ijggc.2019.06.011

Lee, D. S., Allen, M. R., Cumpsty, N., Owen, B., Shine, K. P., & Skowron, A. (2023). Uncertainties in mitigating aviation non-CO_2 emissions for climate and air quality using hydrocarbon fuels. *Environmental Science: Atmospheres*, *3*(12), 1693–1740. https://doi.org/10.1039/D3EA00091E

LeNeveu, D. M. (2008). CQUESTRA, a risk and performance assessment code for geological sequestration of carbon dioxide. *Energy Conversion and Management*, *49*(1), 32–46. https://doi.org/10.1016/j.enconman.2007.06.001

Lu, M., & Connell, L. D. (2014). The transient behaviour of CO 2 flow with phase transition in injection wells during geological storage – Application to a case study. Journal of Petroleum Science and Engineering, 124, 7–18. https://doi.org/10.1016/j.petrol.2014.09.024

Mehana, M., Chen, B., & Pawar, R. (2022). Reduced-order models for wellbore leakage from depleted reservoirs. Proceedings of the 10th Unconventional Resources Technology Conference. Unconventional Resources Technology Conference, Houston, Texas, USA. https://doi.org/10.15530/urtec-2022-3725868

Moeinikia, F., Ford, E. P., Lohne, H. P., Arild, Ø., Majoumerd, M. M., & Fjelde, K. K. (2018). Leakage calculator for plugged-and-abandoned wells. *SPE Production & Operations*, *33*(04), 790–801. https://doi.org/10.2118/185890-PA

Nelson, E. B. (Ed.). (1990). *Well cementing*. Elsevier.

Nicot, J.-P. (2009). A survey of oil and gas wells in the Texas Gulf Coast, USA, and implications for geological sequestration of CO2. *Environmental Geology*, *57*(7), 1625–1638. https://doi.org/10.1007/s00254-008-1444-4

Nordbotten, J. M., Celia, M. A., Bachu, S., & Dahle, H. K. (2005). Semianalytical solution for co_2 leakage through an abandoned well. *Environmental Science & Technology*, *39*(2), 602–611. https://doi.org/10.1021/es035338i

Nordbotten, J. M., Kavetski, D., Celia, M. A., & Bachu, S. (2009). Model for co_2 leakage including multiple geological layers and multiple leaky wells. *Environmental Science & Technology*, *43*(3), 743–749. https://doi.org/10.1021/es801135v

NSTA. (2025). Southern North Sea Regional Geological Maps. https://opendata-nstauthority.hub.arcgis.com/documents/be4c9089a1c04851970ec256695b49b7/about (accessed, February 2025)

Pan, L., & Oldenburg, C. M. (2014). T2Well—An integrated wellbore–reservoir simulator. *Computers & Geosciences*, 65, 46–55. https://doi.org/10.1016/j.cageo.2013.06.005

Pan, L., Webb, S. W., & Oldenburg, C. M. (2011). Analytical solution for two-phase flow in a wellbore using the drift-flux model. *Advances in Water Resources*, 34(12), 1656–1665. https://doi.org/10.1016/j.advwatres.2011.08.009

Pedersen, K. S., Fredenslund, A., Christensen, P. L., & Thomassen, P. (1984). Viscosity of crude oils. *Chemical Engineering Science*, *39*(6), 1011–1016. https://doi.org/10.1016/0009-2509(84)87009-8

Peng, D.-Y., & Robinson, D. B. (1976). A new two-constant equation of state. *Industrial & Engineering Chemistry Fundamentals*, *15*(1), 59–64. https://doi.org/10.1021/i160057a011

Pullen, B., Cahill, A., & Arnold, D. (2025). Differentiating legacy wellbores in the scottish north sea using multi-criteria decision analysis with a view to minimising containment risk for carbon capture and storage. *International Journal of Greenhouse Gas Control*, *142*, 104336. https://doi.org/10.1016/j.ijggc.2025.104336

Ramachandran, H. (2025). QWellRATE: A simplified physics-based model for estimating CO_2 leakage fluxes along legacy wells [Computer software]. Zenodo. https://doi.org/10.5281/zenodo.17485764

Riahi, K., Schaeffer, R., Arango, J., Calvin, K., Guivarch, C., Hasegawa, T., Jiang, K., Kriegler, E., Matthews, R., Peters, G.P. and Rao, A., 2023. Mitigation Pathways Compatible with Long-term Goals (Chapter 3). *IPCC 2022: Climate Change 2022: Mitigation of Climate Change. Contribution of Working Group III to the Sixth Assessment Report of the Intergovernmental Panel on Climate Change*, pp.295-408.

Riddick, S. N., Mauzerall, D. L., Celia, M. A., Kang, M., & Bandilla, K. (2020). Variability observed over time in methane emissions from abandoned oil and gas wells. *International Journal of Greenhouse Gas Control*, *100*, 103116. https://doi.org/10.1016/j.ijggc.2020.103116

Smith, A., Hampson, G., Kivi, I. R., & Krevor, S. (2026). Carbon dioxide plumes, pressure space and legacy well risk for Southern North Sea CO2 storage projects. *Energy Geoscience*, *7*(1), 100475. https://doi.org/10.1016/j.engeos.2025.100475

Span, R., & Wagner, W. (2003a). Equations of state for technical applications. I. Simultaneously optimized functional forms for nonpolar and polar fluids. *International journal of thermophysics*, *24*, 1-39. https://doi.org/10.1023/A:1022390430888

Span, R., & Wagner, W. (2003b). Equations of state for technical applications. II. Results for nonpolar fluids. *International Journal of Thermophysics*, *24*, 41-109. https://doi.org/10.1023/A:1022310214958

Tao, Q., & Bryant, S. L. (2014). Well permeability estimation and CO2 leakage rates. *International Journal of Greenhouse Gas Control*, *22*, 77-87. https://doi.org/10.1016/j.ijggc.2013.12.022

Tao, Q., Checkai, D., Huerta, N., & Bryant, S. L. (2010). Model to predict co2 leakage rates along a wellbore. *SPE Annual Technical Conference and Exhibition*, SPE-135483-MS. https://doi.org/10.2118/135483-MS

Torsæter, M., Bello-Palacios, A., Borgerud, L. K., Nygård, O.-K., Frost, T. K., Hofstad, K. H., & Andrews, J. S. (2024). Evaluating legacy well leakage risk in co2 storage. *SSRN Electronic Journal*. https://doi.org/10.2139/ssrn.5062896

Townsend-Small, A., Ferrara, T. W., Lyon, D. R., Fries, A. E., & Lamb, B. K. (2016). Emissions of coalbed and natural gas methane from abandoned oil and gas wells in the United States. *Geophysical Research Letters*, *43*(5), 2283–2290. https://doi.org/10.1002/2015GL067623

Underhill, J. R., De Jonge-Anderson, I., Hollinsworth, A. D., & Fyfe, L. C. (2023). Use of exploration methods to repurpose and extend the life of a super basin as a carbon storage hub for the energy transition. *AAPG Bulletin*, *107*(8), 1419–1474. https://doi.org/10.1306/04042322097

Vasylkivska, V., Dilmore, R., Lackey, G., Zhang, Y., King, S., Bacon, D., Chen, B., Mansoor, K., & Harp, D. (2021). NRAP-open-IAM: A flexible open-source integrated-assessment-model for geologic carbon storage risk assessment and management. Environmental Modelling & Software, 143, 105114. https://doi.org/10.1016/j.envsoft.2021.105114

Vesovic, V., Wakeham, W. A., Olchowy, G. A., Sengers, J. V., Watson, J. T. R., & Millat, J. (1990). The transport properties of carbon dioxide. *Journal of Physical and Chemical Reference Data*, *19*(3), 763–808. https://doi.org/10.1063/1.555875

Vielstädte, L., Karstens, J., Haeckel, M., Schmidt, M., Linke, P., Reimann, S., Liebetrau, V., McGinnis, D. F., & Wallmann, K. (2015). Quantification of methane emissions at abandoned gas wells in the Central North Sea. *Marine and Petroleum Geology*, *68*, 848–860. https://doi.org/10.1016/j.marpetgeo.2015.07.030

Viswanathan, H. S., Pawar, R. J., Stauffer, P. H., Kaszuba, J. P., Carey, J. W., Olsen, S. C., Keating, G. N., Kavetski, D., & Guthrie, G. D. (2008). Development of a hybrid process and system model for the assessment of wellbore leakage at a geologic co2 sequestration site. *Environmental Science & Technology*, 42(19), 7280–7286. https://doi.org/10.1021/es800417x

Vrålstad, T., Saasen, A., Fjær, E., Øia, T., Ytrehus, J. D., & Khalifeh, M. (2019). Plug & abandonment of offshore wells: Ensuring long-term well integrity and cost-efficiency. *Journal of Petroleum Science and Engineering*, *173*, 478-491. https://doi.org/10.1016/j.petrol.2018.10.049

Yang, Y.-M., Dilmore, R. M., Mansoor, K., Buscheck, T. A., & Bromhal, G. S. (2019). Integration of wellbore pressure measurement and groundwater quality monitoring to enhance detectability of brine and CO2 leakage. *International Journal of Greenhouse Gas Control*, *85*, 143–155. https://doi.org/10.1016/j.ijggc.2019.04.004

Zhang, M., & Bachu, S. (2011). Review of integrity of existing wells in relation to CO2 geological storage: What do we know? *International Journal of Greenhouse Gas Control*, *5*(4), 826–840. https://doi.org/10.1016/j.ijggc.2010.11.006

Zhang, Y., Oldenburg, C. M., Finsterle, S., & Bodvarsson, G. S. (2007). System-level modeling for economic evaluation of geological CO2 storage in gas reservoirs. *Energy Conversion and Management*, *48*(6), 1827–1833. https://doi.org/10.1016/j.enconman.2007.01.018

Zheng, L., Carroll, S., Bianchi, M., Mansoor, K., Sun, Y., & Birkholzer, J. (2014). Reduced order models for prediction of groundwater quality impacts from co2 and brine leakage. Energy Procedia, 63, 4875–4883. https://doi.org/10.1016/j.egypro.2014.11.518

Zhou, W., Stenhouse, M., Arthur, R., Whittaker, S., Law, D., Chalaturnyk, R., & Jazrawi, W. (2005). The IEA Weyburn CO2 monitoring and storage project—Modeling of the long-term migration of CO2 from Weyburn. In *Greenhouse Gas Control Technologies 7: Vol. I* (pp. 721–729). Elsevier. https://doi.org/10.1016/B978-008044704-9/50073-2